QUASI-STATIC COMPRESSION OF GRANULAR MATERIALS

(SAND) AT HIGH PRESSURES ($\sim$ 3 GPA)

By

VIJAY KRISHNAN SUBRAMANIAN

Bachelor of Engineering in Mechanical
Anna University
Chennai, Tamil Nadu, India
2005

Submitted to the Faculty of the
Graduate College of
Oklahoma State University
in partial fulfillment of
the requirements for
the Degree of
MASTER OF SCIENCE
December, 2010

COPYRIGHT ©

By

VIJAY KRISHNAN SUBRAMANIAN

December, 2010

QUASI-STATIC COMPRESSION OF GRANULAR MATERIALS

(SAND) AT HIGH PRESSURES ($\sim$ 3 GPA)

Thesis Approved:

Dr. Ranga Komanduri, Thesis Advisor

Dr. Raman P. Singh

Dr. Sandip Harimkar

Dr. Gordon Emeslie, Dean of the Graduate College

ACKNOWLEDGMENTS

I thank my advisors, Professor Ranga Komanduri and Professor Hongbing Lu for providing me with the opportunity to work on the project on the mechanics of granular materials. It is their continued support, motivation, and patience that has helped me to overcome the barriers and successfully advance in this study. My special thanks to Dr. Komanduri for his support and advise at times of need. I thank Dr. Lu for mentoring and motivating me with his discussions on approach to scientific study.

My special thanks are due to Dr. William Cooper of Air Force Research Laboratory, Eglin Air Force Base for sharing his valuable time and thoughts during the lively discussion sessions.

I would like to thank the School of Mechanical and Aerospace Engineering (MAE) for their support and facilities that has enabled me to conduct the research presented in this thesis.

I thank Dr. Huiyang Luo for sharing his experience in the design and experimentation. His suggestions and feedbacks have helped me throughout my study. I thank Dr. Rutuparna Narulkar and my graduate

colleagues Chetan Kulkarni, Yao Ren , Boshen Fu, Upendra Phatak and Aravind Seshadri for their help and support. I thank Sarah Staggs for providing the SEM scans on Eglin sand.

I thank Gary Thacker (Manager, Advanced Technology and Research Center (ATRC)), Jerry Dale (Manager (retired), ATRC), John Gage (Manager, Design Manufacturing Lab), Ron Markum (Engineer, Web Handling Center) and Mike Lucas (Manager, Instrument/Maintenance Shop in the Department of Physics) for their help in designing and fabrication of the apparatus used in this study.

I express my countless thanks to my dear parents, Subramanian Krishnamurthy and Uma Subramanian, for their unconditional love, support, patience and encouragement that has helped me stay motivated throughout my study. I also thank my dear sister, Revathy Subramanian, for her love and support.

Finally, I would like to thank the Department of Defense (AFOSR) for funding this project through DEPSCoR grant FA9550-08-1-0328.

TABLE OF CONTENTS

LIST OF TABLES

LIST OF FIGURES

CHAPTER 1

INTRODUCTION

Granular materials are agglomerates of discrete macroscopic particles, which respond to external forces only when interlocking takes place at the points of contact. They resemble solids as they behave rigidly in compression due to grain interlocking. Due to discrete and unbonded nature of the grains, they cannot withstand load under tension. When the interlocking between the grains collapse, they lose resistance to shear loading and exhibit flow behavior similar to that of liquids. The solid-liquid transitional behavior of granular materials can be observed in grains stored in silos to landslides. They resemble liquids by taking the shape of the container that they are stored. They resemble gases as they lack intergranular cohesion. Jaeger *et al.* [19] describe granular materials as "unusual" solids, liquids or gases. They describe granular materials as a unique state of matter. The study of granular materials is currently active in various fields of engineering and sciences; including physics, geophysics, mechanics, and pharmacy.

Table 1.1: USCS classification of soil types and grain sizes. (ASTM D2487) [1]

Soil type	**Description of soil**	**Average Grain size**
Gravel	Rounded to angular shape, hard rock.	*Coarse*: 19 mm to 75 mm *Fine*: 4.75 mm to 19 mm
Sand	Rounded to angular shape, hard rock.	*Coarse*: 2 mm to 4.75 mm (Sieve#10) *Medium*: 0.425 mm to 2 mm (Sieve#40) *Fine*: 0.075 mm to 0.425 mm (Sieve#200)
Silt	Little to no strength when dried.	0.002 mm to 0.075 mm
Clay	Exhibits strength when dried.	$<$0.002 mm

Sand is a granular material abundantly found in nature. It is formed by the erosion of rocks and minerals over a long period of time. Unified Soil Classification System (USCS) [1] categorizes soil in to four main types, namely, gravel, sand, silt and clay; in the order of decreasing particle size. Sand is identified by its hard structure and particle size varying between 7.5 μm and 4.75 mm as shown in Table 1.1 (pg. 2). Sand primarily consists of silicon dioxide (SiO_2) while other constituents, such as magnetite, gypsum, chlorite are present and vary from one geographic location to the other. Sand is usually described by their morphology (shape), size, color and texture. Figure 1.1 (pg. 3) show the SEM images of sand grains exhibiting grain shapes, rounded edges, surface features such as fracture facets and pits.

Mechanical behavior of sand has been of interest to civil and military

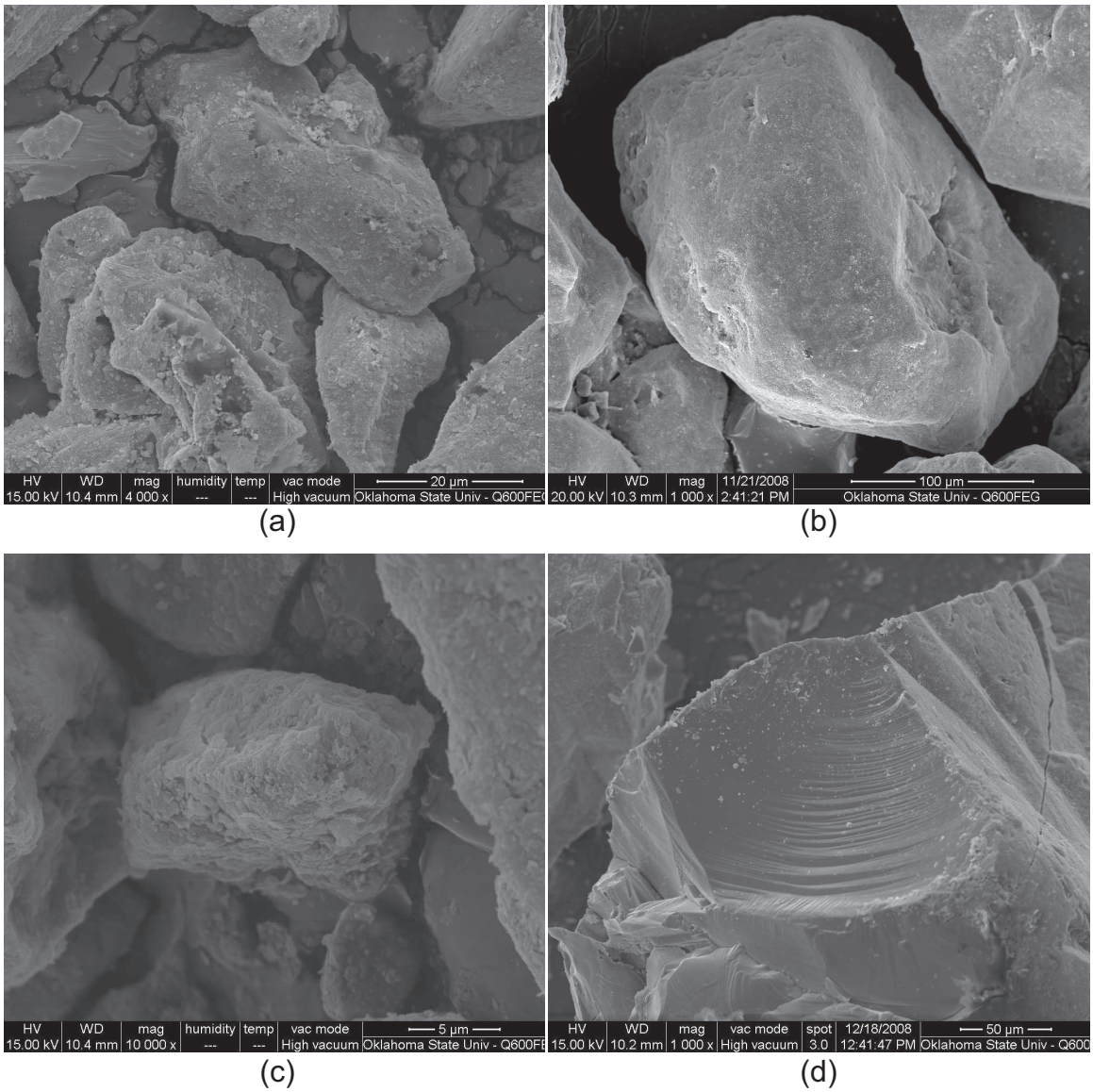

Figure 1.1: SEM images of sand grains at various magnifications showing grain shapes, rounded edges and surface features such as cracks and pits, fracture akin to glass fracture.

engineering. Numerous studies on the penetration of projectiles in sand have been conducted to understand and predict the behavior of projectiles in sand. Other studies on sand surround activities such as mining, drilling of deep wells for oil extraction, construction of sand embankments, packing of nuclear fuels, and structures to withstand explosions. Unlike metals, which have been extensively studied and their behavior successfully modeled in view their continuum nature, granular materials still remain a challenge [2, 3, 5, 19]. Bulk modeling based on continuum assumption of granular materials requires involvement of additional factors, such as grain contact, fracture, friction and heterogeneity in shape and particle sizes. Extensive experimental characterization of the sand behavior under different conditions would be required to develop meaningful constitutive models. The current lack of such constitutive laws for granular materials shows the complexity of modeling the static as well as dynamic behaviors of sand. Various factors have been identified to influence the behavior of sand including initial packing density, size and shape of the grains, strength of individual grains, moisture content, confining pressures, loading rate etc. This investigation focuses on the effects of initial packing density, grain size, and moisture content at low strain-rates (less than 10^{-3} s^{-1}) on the compressive behavior of sand under axial pressures up to 3 GPa, which is close to its crystal yield strength.

1.1 Layout of the Thesis

The thesis is organized as described in the following.

Chapter 2 deals with a review of the literature in one-dimensional quasi-static behavior of sand. Although sand has been studied for well over eight decades, much of the early work in the compressive behavior was restricted to low pressures (below 138 MPa). High pressure investigations on sand began in 1990s. The effect of grain shape, size, density and moisture content on the compression behavior of sand has been presented. Unconfined compression tests on sand is not possible in view of the fact that sand grains are loosely held and hence studies on sand have been conducted using confinements. A cylindrical confinement or a triaxial apparatus was used to provide confinement pressures. The results of such investigations are discussed in this chapter.

Chapter 3 describes the experimental technique involves in confined compression. Schematic of confined compression technique and equations used to derive the constitutive properties of the material being tested are described in this chapter.

Chapter 4 presents the problem statement of the thesis. Based on the review of literature on the compressive behavior of sand and the technique of confined compression, the problem statement is defined. The parameters influencing the behavior of sand are chosen and investigated at

high pressures in this study.

Chapter 5 describes the experimental setup designed and used in the confined compression testing of sand. Method of preparation of the samples, details on the design of the experimental fixture, procedures followed during the tests, and special considerations are also described in this chapter.

The results of confined compression tests on Eglin sand are presented in Chapter 6. The parameters influencing the behavior of sand, namely, initial packing density, grain size and moisture content have been investigated. Plots of axial stress versus strain, radial stress versus axial strain for different parameters are presented. The derived hydrostatic and deviatoric stresses are also presented and discussed.

Chapter 8 summarizes the findings of this investigation. Based on the results and conclusions, suggestions for future work is outlined.

CHAPTER 2

LITERATURE REVIEW

Due to the abundance of sand on the earth's crust, it continues to be an important part of man's activities. Industries such as mining, agriculture, construction, and manufacturing deal with sand apart from other granular materials. Sand in the mine shafts and earthen dams experience pressures of 7 MPa whereas deep well shafts experience pressures of up to 70 MPa [32]. Pile foundations exert pressures of 350 MPa in the soil under the tips of the pile drivers [24]. Models developed to describe the compressive behavior of sand are valid at low pressures and have been validated at pressures below 100 MPa. Sand has been observed to undergo higher stresses in cases of projectile penetrating in sand [2, 3], explosion sites [18], and even packing of spent nuclear fuels in pressurized containers [12]. This chapter presents a review of previous investigations on sand beginning from 1920s. Much of the initial studies on soil was done by Karl Terzaghi for which he is known as the father of soil mechanics. His studies and reports laid the foundations for much of the soil mechanics developed to date.

Some of the initial work on the compressive behavior of sand was reported by Blackwelder in 1920 [4]. In his study on the formation of oil domes in Central Kansas and Northern Oklahoma, he cited the lack of experimental data on the condensation behavior of various kinds of sediments under different loading levels. He observed that clean sand was relatively incompressible at "ordinary loads" as compared to silt and clay, which are easily compressed to 50% of their initial volume. He noticed no crushing of the sand grains in the domes.

Based on a series of studies on sand and clay Terzaghi [27] reported, in 1925, the elastic properties of sand confined in a steel ring and compressed to different pressures. From the tests, he found that the stress-strain curve of compacted sand to be less steeper than that of loose sand as shown in Figure 2.1 (pg. 9). He observed no significant crushing of sand grains at 4.9 MPa. Terzaghi defined the term "Coefficient of lateral earth pressure at rest" (K_0) as the ratio of total horizontal soil pressure (σ_h) to the vertical soil pressure (σ_v), as shown in Equation 2.1. The coefficient of lateral earth pressure at rest is used to describe the stress state in the soil. In 1948, Jaky developed the relationship between K_0 and Mohr-Coulomb angle of internal friction (ϕ) as shown in Equation 2.2.

$$K_0 = \frac{\sigma_h}{\sigma_v} \tag{2.1}$$

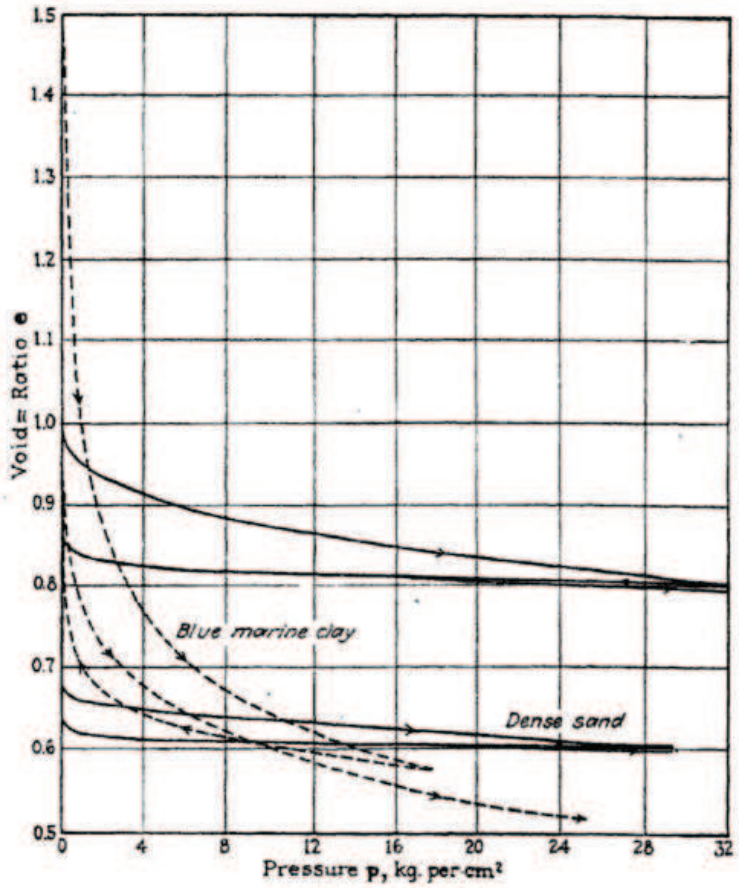

Figure 2.1: Pressure-void ratio curves for sand and clay, show stiffer response from sand. (after Terzaghi *et al.* [27])

$$K_0 = 1 - sin\phi \tag{2.2}$$

In 1935, Botset and Reed [6] pointed out that previous test results on compressibility of sand were influenced by the stiffness of the confining cylinder. They developed an apparatus for measuring the compressibility of sand by measuring the volume of liquid ejected forcefully by sand when it was compressed. This volume of ejected liquid was used to determine the change in the volume of the pores. In their tests, a maximum stress

of 20 MPa was attained. Sieve analysis of the sand samples after testing showed at least 8% crushing of sand grains. Multiple loading cycles showed non-coincident loading paths. They concluded that the crushing of sand grains was the underlying phenomenon for the non-coincident loading behavior.

In 1948, Terzaghi and Peck [28] observed particle crushing in their sand tests at stresses of up to 96 MPa. This work was followed by a series of investigations aimed at the phenomenon of particle crushing. In 1958, DeSouza [10] conducted tests on sand at an axial pressure of 137 MPa. They observed a change in the displacement beyond a critical pressure. The "critical pressure" was found to be influenced by the initial packing density. They found an increase in particle crushing after the pressure exceeds the "critical pressure". They also found the angular shaped sand grains to show higher compressibility as compared to rounded grains. In 1959, Harremoes [16] conducted compression tests on sand obtained from Ottawa sand and Hawaiian beaches, up to pressures as high as 138 MPa. He concluded that crushing of different types of sand particles occurred at similar "critical pressures" as that reported by Desouza.

In 1957, Allen *et al.* [2, 3] conducted projectile penetration tests on sand to experimentally verify the validity of the projectile penetration models. In their projectile penetration tests on sand confined in a box, they found that the projectile had left behind a trail of powdered sand. They explained

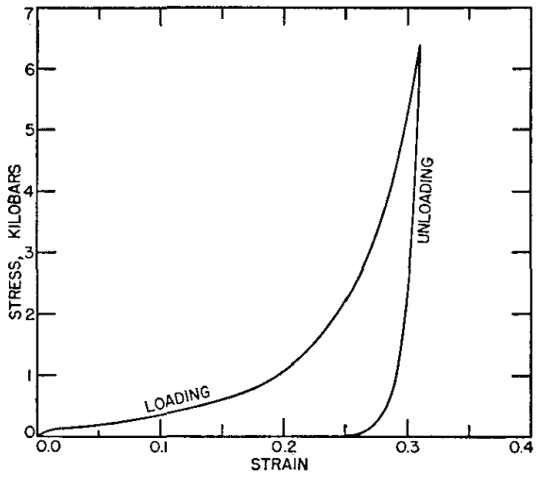

Figure 2.2: Stress-strain curve for confined sand obtained from the static compression tests by Allen *et al.* [2]

that crushing of sand grains allowed the projectile to move forward, which otherwise is resisted by the binding of sand grains. In order to determine the stress levels experienced by the sand projectile as it decelerated through the sand medium. Static tests were conducted to observe the extent of grain crushing as a function of axial stress. Sand was confined in a steel cylinder and compressed to a maximum axial stress of 600 MPa. They observed the onset of grain crushing to occur at 10 MPa, which was marked by the "knee of the loading curve", as shown in Figure 2.2 (pg. 11). This was considered to be the threshold value for comminution of sand grains. This work spurred interest in the studies on static and dynamic response of sand in order to understand and predict the depth and trajectory of projectiles penetrating into sand.

In 1963, Hendron [17] reported a series of uniaxial compression tests

aimed at studying the effect of initial density of various sands on the stress-strain behavior. Sand from various sources, namely, Minnesota, Pennsylvania, Sangamon river and Wabash river were confined in a thin steel ring. He studied the influence of initial relative density on the stress-strain behavior of sands. He found that denser sand produced a steeper stress-strain curve as compared to less dense sand sample. The constrained tangent modulus of deformation, defined as the rate of change of vertical stress to the vertical strain at zero lateral strain, was found to increase with increase in the initial relative density. The stress levels at which sand crushing occurred increased as the initial density increased. He attributed this behavior to the ability of less dense sand to rearrange to a greater extent, preventing the early onset of cracking. The average stress levels at which cracking of sand grains occurred was found to be significantly higher with increasing initial density.

Hendron [17] also found that the angularity of sand grains was a significant factor as the initial density. Rounded sand particles tend to show a stiffer loading behavior and higher strain recovery during unloading. He predicted that the physical properties exhibited by sand of various initial densities might eventually merge into a single curve at higher pressures, which was beyond the ability of his test apparatus. He laid out the mechanism for energy absorption in uniaxial compression of sand at high pressures to be arising from: (a) the rearrangement of grains leading to permanent reduction in volume, (b) the crushing of the grains

leading to the creation of new surfaces, and (c) friction between the grains causing elastic hysteresis in strains. Hendron postulated that the larger extent of crushing in bigger sand grains occurred due to increased inter-particle stresses which vary inversely with particle size. The extent of moisture content in sand was found to be a significant factor in altering its behavior. Tests performed on different levels of moisture in sandy silt at various densities found that the stiffness of the stress-strain curve increased as moisture content increased.

Testing of unconfined sand is not possible. The influence of confinement on the strength of sand has been acknowledged quite early [6]. Researchers assumed different geometries and materials of the confinement to be suited for their investigations on sand. There was no clear method of measuring the pressures exerted by the confinement. With the advent of triaxial testing apparatus, axial compression tests could be conducted at pre-determined confinement pressures which is maintained constant through the test. The triaxial apparatus has thus become a standard testing method for investigating geomaterials.

Figure 2.3 (pg. 15) shows a schematic of a conventional triaxial test apparatus used for testing sand. The principle of triaxial testing is to maintain constant lateral pressures on the specimen independent of the applied axial stresses. This permits a multiaxial stress state to be imposed on the specimen. Axial stress-strain measurements on the specimen are

obtained for a constant lateral (confining) pressure. The apparatus consists of a pressurized fluid cell in which the test specimen is placed in a sealed elastic membrane, usually rubber. The elastic membrane allows the specimen to deform freely. Axisymmetric (cylindrical) specimen is to maintain uniform lateral pressures. The desired confinement pressures are obtained by controlling the pressure of the fluid pressure. The pressurized cell containing the specimen is compressed in an uniaxial test frame. As the applied axial stress exceeds the radial pressure, the sample undergoes vertical compression. The applied axial stress (σ_1) and the radial stress (σ_3) are the principle stresses. The total applied stress is $\sigma_1 = \frac{P}{A_s} + \sigma_3$ and the deviatoric stress is $\sigma_1 - \sigma_3$. The angle of internal friction can be determined by $\phi = sin^{-1}\frac{\sigma_1 - \sigma_3}{\sigma_1 + \sigma_3}$. The triaxial setup is useful in the determination of stress-strain behavior as well as the shear behavior of sand.

In 1963, Hall and Gordon [14] investigated the effect of particle size distribution using triaxial tests up to 4.5 MPa. They found that well-graded sands showed less crushing at the same stress levels as compared to poorly graded ones.

In 1968, Vesic and Clough [30] reported the results of a series of triaxial tests in which the maximum confinement pressures reached 69 MPa (10,000 psi), which they call as high pressures. They cited the need for triaxial testing of sands at pressures exceeding 6.9 MPa (1,000 psi) to help predict soil behavior in deep wells, tunnels, and nuclear blast sites. They

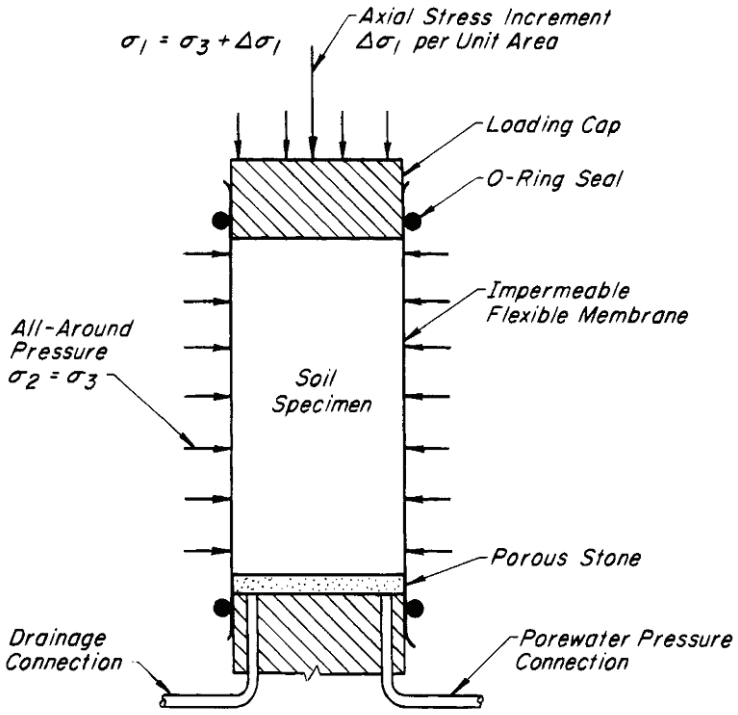

Figure 2.3: Schematic of a triaxial apparatus for testing sand, (after Terzaghi *et al.* [28].

designated the pressures below 6.9 MPa to be low pressures. Their tests were aimed at verifying the validity of extending the behavior of sand based on low pressure tests to higher pressures. Based on their tests, they reported that dense sand behaved differently at higher pressures than at lower pressures. Below 1 MPa, they observed very little crushing and the dilatation was pronounced, due to the ability of sand grains to rearrange. Crushing of grains intensified between 1 MPa and 10 MPa.

Vesic and Clough [30] defined "breakdown stress" as the axial stress required to eliminate all the effects of initial void ratio. Upon reaching

the "breakdown stress" the particle crushing was minimal. Above the breakdown stress, they observed that sand essentially behaved as rigid deformable solid, characterized by a modulus of deformation. The angle of internal friction (ϕ) decreases inversely with mean normal stress at low pressures, until the breakdown stress was reached. Above the breakdown stress, ϕ was found to remain constant. Further, they speculated the behavior of sand at pressures beyond 69 MPa and as high as 10 GPa, to undergo one more change as the porosity reached low values close to zero. The limitations of triaxial apparatus in reaching pressures above 100 MPa prevented the extension of their tests to higher pressures. The difficulty in the design and implementation of high pressure cells and loss of impermeability in the membrane separating the specimen from the oil impose practical limitations to the range of testing pressures achieved in triaxial testing.

In 1993, Hagerty *et al.* [13] reported the results of investigations on one-dimensional compression of sand for maximum axial pressure of 689 MPa (100,000 psi). Their primary objective was to reach higher stresses, above 138 MPa (10,000 psi). Tests were conducted at high pressures to investigate the effect of initial packing density, angularity of particles, and particle mineralogy.

The experimental setup of Hagerty *et al.* [13] consisted of a steel confining ring with an outer diameter of 203 mm (8 in.) and an inner

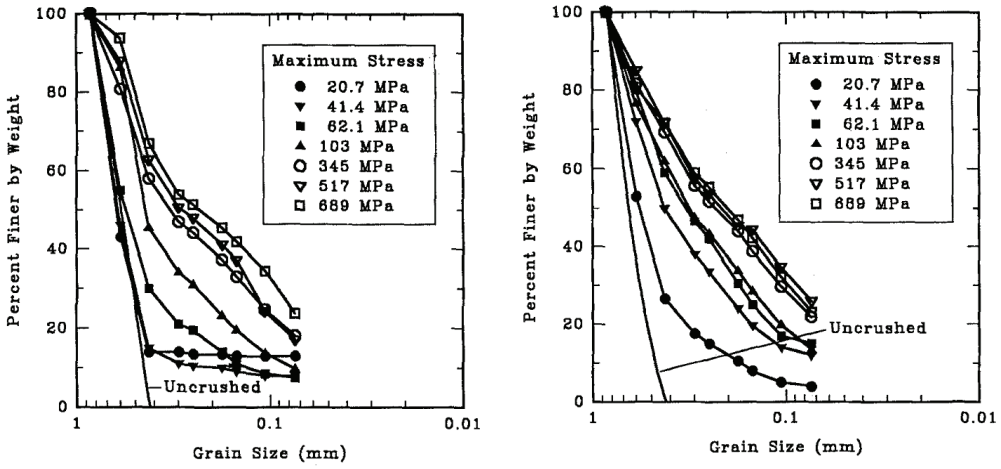

Figure 2.4: Grain size distributions for the Ottawa sand (rounded) and Black Beauty sand (angular) at different axial stresses showing the extent of particle crushing with increased axial stresses. (after Hagerty *et al.* 1993 [13])

diameter of 75.4 mm (2.97 in.). The specimen was placed in a ring and steel loading cap was placed on top of the ring. This setup was then placed in the uniaxial testing frame and compressed statically to stresses of 34.5 MPa (5,000 psi), 103 MPa (10,000 psi), 345 MPa (15,000 psi), 517 MPa (20,000 psi), and 689 MPa (25,000 psi). The tests were followed by sieve analysis to investigate the extent of grain crushing at different stress levels. Ottawa sand (uniform size and rounded shape), Black Beauty slag (angular in shape) and glass beads were used for the tests.

Figure 2.4 show the results of grain size distribution for different axial stresses exerted on the Ottawa sand and Black Beauty slag. The spherical Ottawa sand exhibited less particle crushing than the angular Black Beauty and glass beads. The Ottawa sand showed higher degree of crushing than

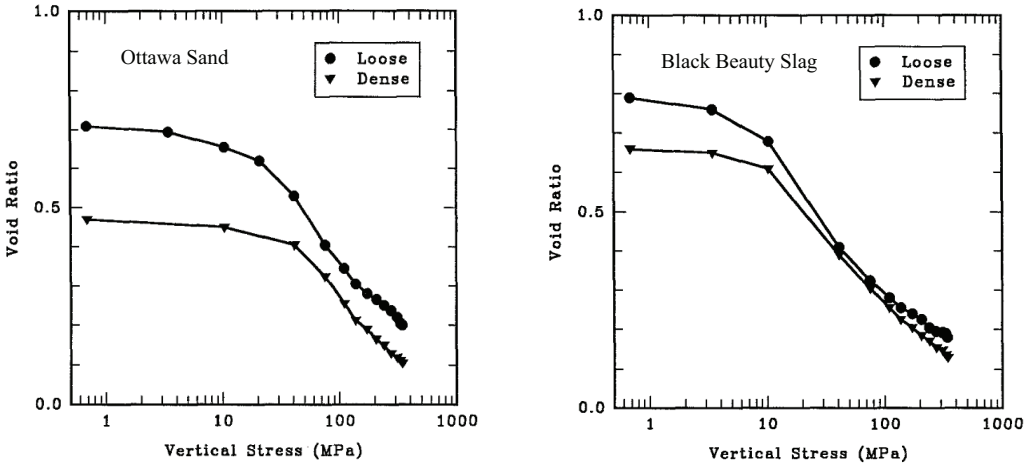

Figure 2.5: Variation of void ratio with vertical stress plots of dense and loose sands. The softer Ottawa sand shows higher degree of crushing when compared to the Black Beauty slag. (after Hagerty *et al.* [13])

the similarly composed glass beads, shown in Figure 2.5 (pg. 18). Hagerty *et al.* noted that Ottawa sand being softer when compared to glass beads, showed greater tendency to fracture which could not be explained. The plots of void ratio vs axial stress indicate the presence of negative void ratio values at higher stresses, which was thought to be due to compression of the mineral particles. Instead, they chose presenting the data in terms of axial stresses vs axial strains. The onset of crushing was detected from the change of initial loading slope in the axial stress- strain curve. This onset of crushing was called the 'crushing stress', denoted by p_c and the slope was called the initial Moduli, denoted by M_i.

Hagerty *et al.* [13] proposed a generalized schematic for the stress-strain behavior of sand particles, shown in Figure 2.7 (pg. 20). The figure shows three distinct phases in the compression of sand. The initial phase,

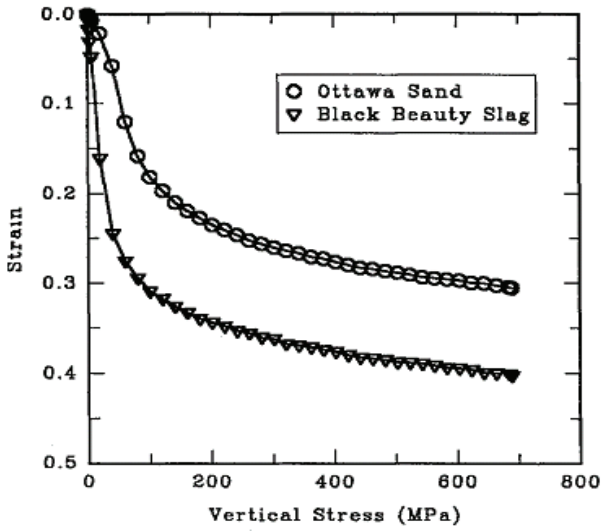

Figure 2.6: Axial stress-strain plots of Ottawa sand and Black Beauty slag showing the similarity in the final moduli. (after Hagerty *et al.* [13])

marked by a secant modulus, was defined as the onset of particle crushing. Phase two that followed the initial onset of particle crushing, comprised of particle crushing and particle redistribution. Further crushing occurred as the stresses increased. This phase showed a drastic drop in the slope with increasing stresses. The third phase, marked by a rapid rise in the slope, occurred as the particle rearrangement and crushing terminated with reduction in void ratio. Crushing decreased and approached a "pseudoelastic" phase. They concluded that the particles showed significant crushing above axial stresses of 138 MPa, which was the limit of previous uniaxial and triaxial studies. The final moduli of dissimilar sands with different grain sizes, shapes, and mineralogy approached a similar value at higher pressures as shown in Figure 2.6.

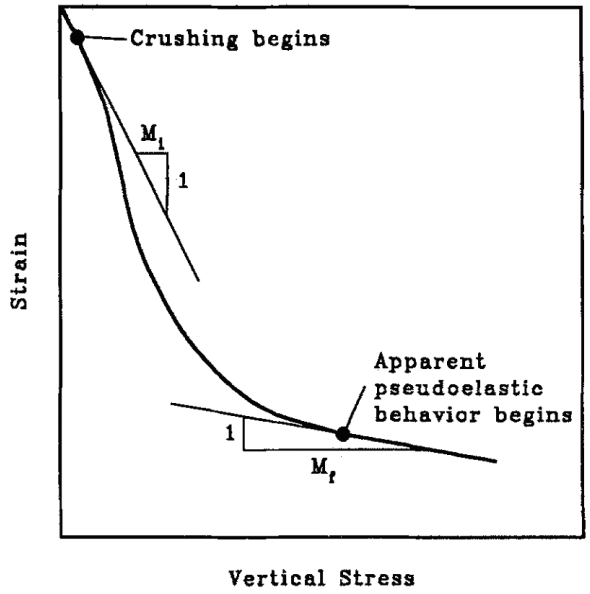

Figure 2.7: Schematic plot of the three phases of compression of sand: particle crushing, redistribution and pseudoelastic phases. (after Hagerty *et al.* [13])

Yamamuro *et al.* [32] performed one-dimensional tests on sand attaining axial stresses up to 850 MPa. Three different types of sands, namely, quartz, Cambria, and gypsum were chosen for their varying mineral hardness of the sand particles. The quartz sand was the hardest and gypsum sand the softest. Cambria sand consisted of particles with hardness ranging from quartz to gypsum. They conducted tests on three different densities for each sand type. Figure 2.8 (pg. 22) shows the schematic of the test cell. It consisted of a hardened steel containment cell to hold the sand sample which was compressed by a piston. Two strain gages were mounted on the surface of the containment in half-bridge configuration to measure the circumferential strain. Axial stress of 850 MPa was attained on all tests and the resulting axial strains were compared. Figure 2.9 (pg. 23) shows the axial stress vs axial strain response of the quartz and gypsum sands. Sand specimens with higher initial density attained the maximum axial stress within smaller axial strains as compared to the less dense specimen. The high stress portions of the curves appeared identical. The softer gypsum sand exhibited large axial strains when compared to the harder quartz sand. The hardness of the sand particles influenced the stress-strain behavior, wherein the harder grains failed by fracture whereas the softer grains exhibited high plastic behavior. In the case of Cambria sand, the soft grains were observed to deform plastically around the harder ones. The void ratios of softer grains experienced highest reduction, almost close to zero.

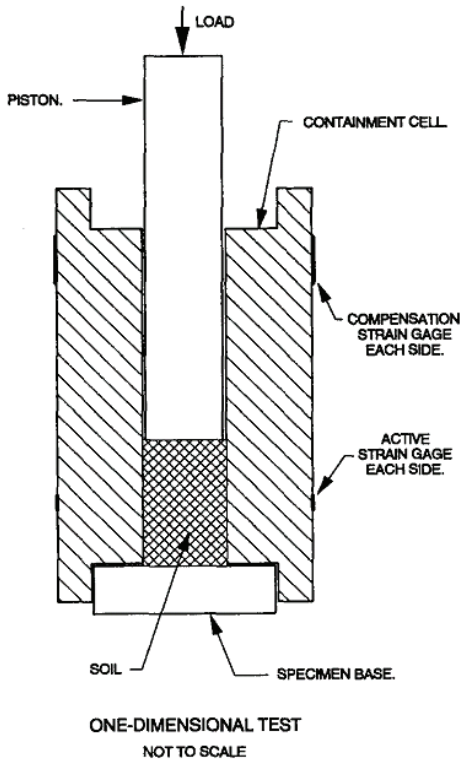

Figure 2.8: Schematic of one-dimensional compression testing apparatus comprising of containment cylinder and piston arrangement to compress sand specimen to 850 MPa axial pressures. (after Yamamuro *et al.* [32])

In all the sand types tested, the effect of initial density on the reduction of void ratio with increasing stress diminished as the void ratio curves merged, as shown in Figure 2.10 (pg. 24). For harder Qaurtz sands, the void ratio curves merged at higher axial stresses. The radial stresses were derived from circumferential strain measurements. In the radial stress vs axial stress plot, (refer to Figure 2.10), the loading portion was observed to be linear while the unloading portion showed a curvature, particularly at lower stress values. The radial stresses were higher for softer (gypsum)

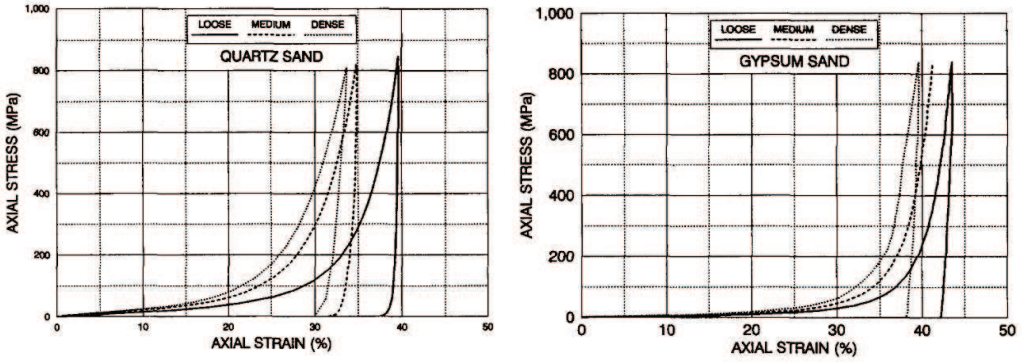

Figure 2.9: Axial stress vs axial strain plots of one-dimension compression of quartz and gypsum sands, showing the effect of density on the stress-strain behavior of sand. (after Yamamuro *et al.* [32])

sand due to plastic yield flow. The presence of moisture contributed to higher radial stresses arising from increased pressures in pores trapped with water. Tests were conducted on the sands with moisture and the effect of moisture on the stress-strain behavior was found to be negligible at higher stresses.

In 1994, Veyera [31] reported the influence of moisture content on the behavior of sand in high strain-rate conditions. Different degrees of saturation in confined sand was tested on the Split Hopkinson Pressure bar (SHPB). Three different sans were tested, namely, Eglin sand, Tyndall sand and Ottawa sand. The sands were chosen for their difference in shape and size distributions. Eglin sand is angular in shape with medium to fine grain size. Ottawa sand is rounded and uniformly graded. Tyndall sand fine and uniform in size with sub-angular shape. The effect of degree of saturation on the dynamic stress-strain behavior of the sands tested are

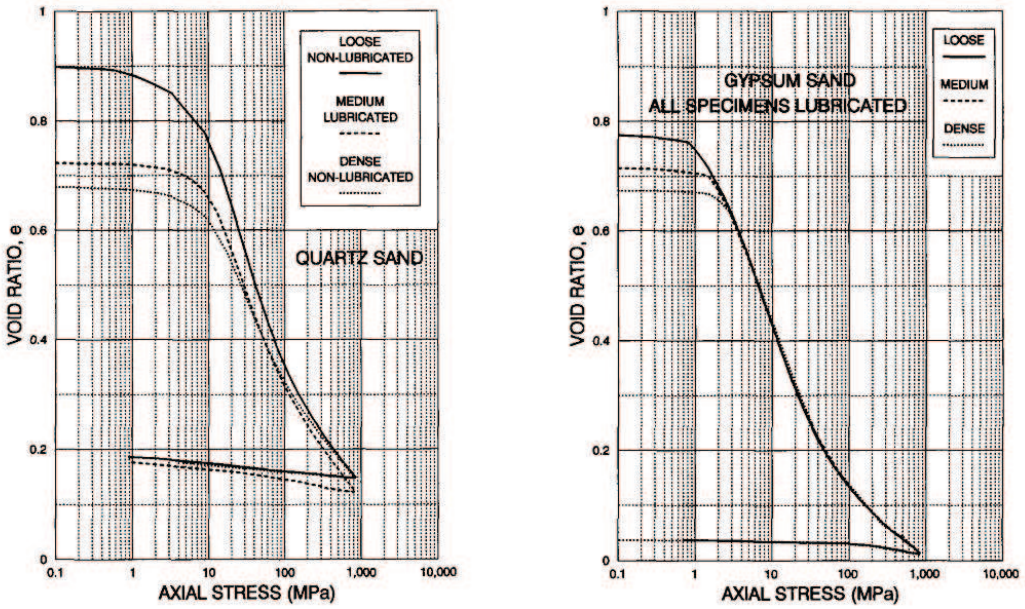

Figure 2.10: Void ratio vs axial stress plots of one-dimension compression of quartz and gypsum sand, showing the effect of grain hardness on the void ratio. (after Yamamuro *et al.* [32])

shown in Figures 2.12- 2.14. The overall effect of moisture on the behavior of sand is marked by the increases in stiffness of the stress-strain curves. The effect of moisture was most observed in Eglin sand while Ottawa sand showed the least change in stiffness. Veyera attributed the differences to the particle size and distribution of sand grains. After an initial sharp rise in the slope, which he termed as the "lock-up", the behavior was found to be dominated by the water phase. The phase until lock-up was dominated by the initial packing condition.

Static and dynamic tests investigating the effect of moisture on the mechanical properties of sand were reported by Martin *et al.* [23]. The static tests were conducted on a uniaxial strain apparatus. Partially saturated

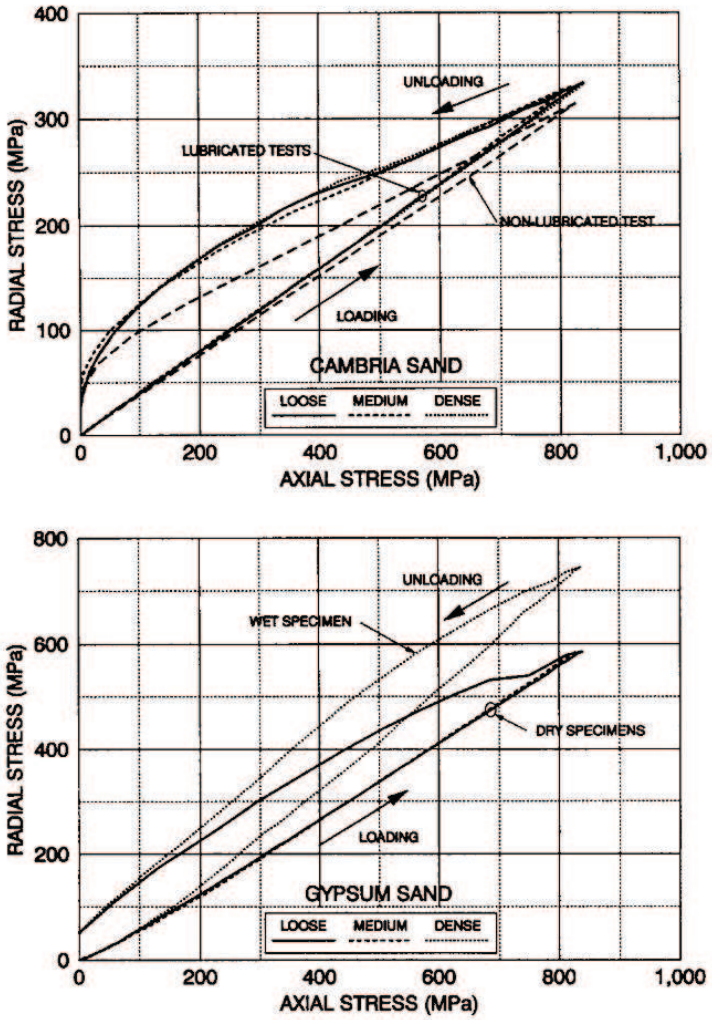

Figure 2.11: Radial stress vs axial stress plots of one-dimensional compression of Cambria and gypsum sands showing linear loading portion and curved unloading portion. The radial stresses were higher for softer (gypsum) sand due to plastic yield flow. The presence of moisture contributed to higher radial stresses arising from increased pressures in pores trapped with water. (after Yamamuro *et al.* [32])

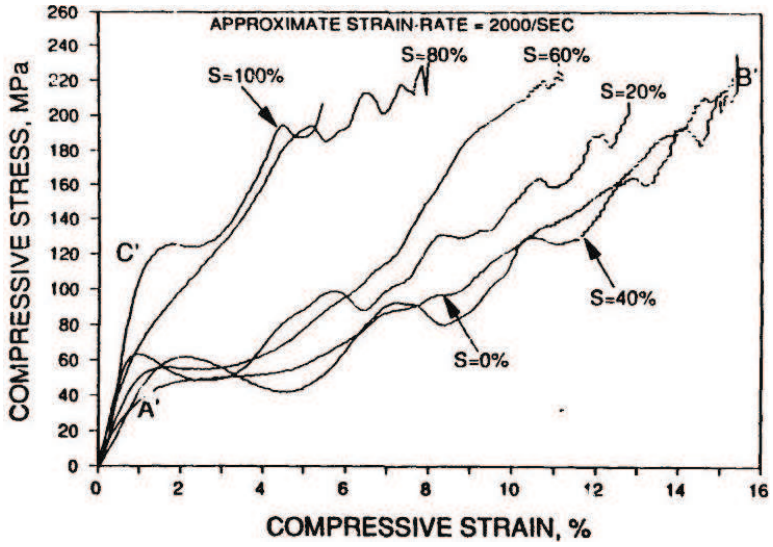

Figure 2.12: Stress-strain curves for Eglin sand at various degrees of water saturation showing increase in slope with increase in moisture content. (after Veyera [31])

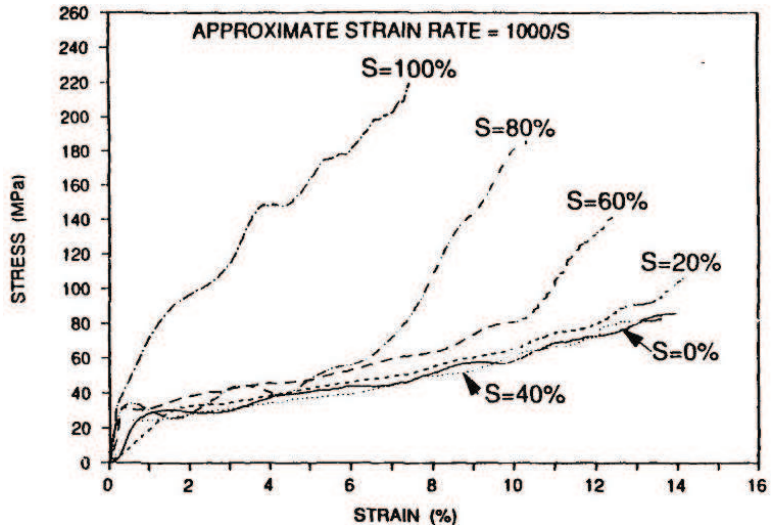

Figure 2.13: Stress-strain curves for Tyndall sand at various degrees of water saturation showing increase in slope with increase in moisture content above 40% saturation. (after Veyera [31])

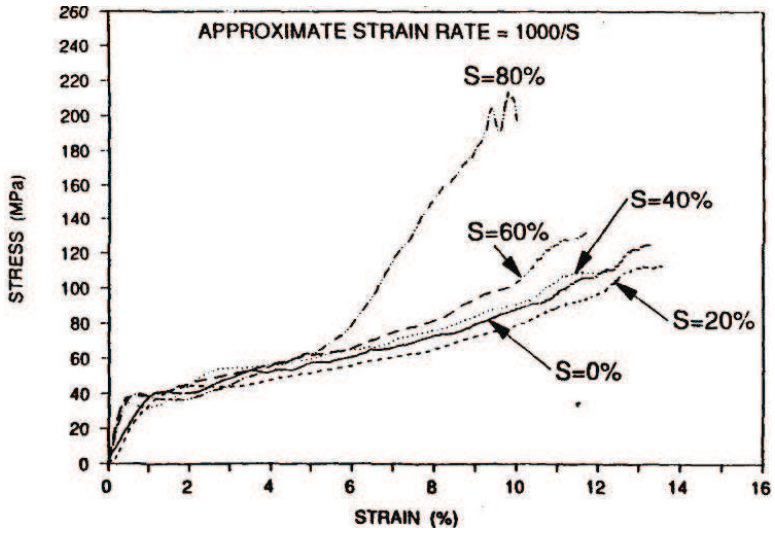

Figure 2.14: Stress-strain curves for Ottawa 20-30 sand at various degrees of water saturation showing small change in slope with increase in moisture content in the 0 to 60% range of water saturation. (after Veyera [31])

sand exhibited less stiffness when compared to dry sand in the axial stress-strain tests. Dynamic tests on SHPB showed similar trend of decreasing stiffness with increase in the moisture content, as shown in Figure 2.15. The softening of grain behavior in sand is explained by the reduction of friction suspected to be caused by the lubricating effect of water between the grains of sand.

The review of literature identified the primary factors influencing the behavior of sand, namely, initial density, grain size, grain shape, mineralogy, and moisture content. Effect of strain rate on the stress-strain behavior was also seen. Densely packed sand exhibited stiffer axial stress versus strain response as compared to loosely packed ones. Sand specimens with higher initial density attained higher stresses within

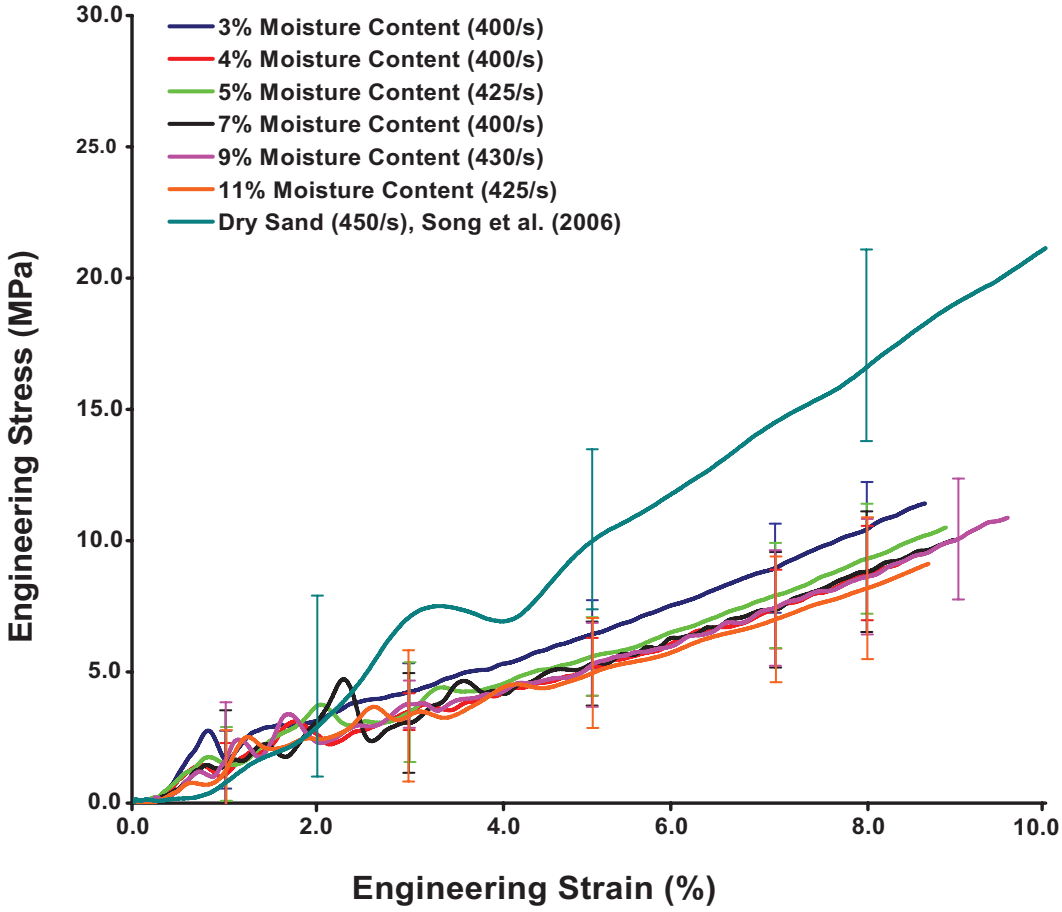

Figure 2.15: Stress-strain curves from dynamic tests on sand with different levels of saturation. (after Martin [22])

smaller axial strains. Harder sand is understood to exhibit failure by fracture whereas softer sand exhibited failure by high plastic deformation. Dynamic tests on the effect of moisture on the stress-strain behavior of sand showed conflicting observations. Veyera [31] reported an increase in stiffness with increase in moisture content due to increase in pore pressures from trapped water in the voids, while Martin **??** reported an decrease

in the stiffness of the axial stress-strain curve due to grain softening and lubrication effect of water.

CHAPTER 3

TECHNIQUE FOR CONFINED COMPRESSION

This chapter describes the testing technique of confined compression used in the characterization of materials. The description of the technique is followed by the equations used to obtain the constitutive properties of the material being tested.

3.1 Method of Confined Compression

Compression testing is widely used to characterize the mechanical behavior of materials. This involves uniaxial loading of the material specimen and measuring the stress-strain response as the specimen deforms homogeneously. Materials undergoing small deformation rarely pose a challenge to the condition of homogeneous deformation. However, materials which undergo large, inelastic deformations exhibit strain localizations in the form of bulging, shear banding, buckling and barreling. Many materials also exhibit pressure sensitive behavior, where the magnitude of hydrostatic pressure acting on the sample influences the mechanical

behavior of the material. Such materials are usually tested using triaxial compression tests. Lateral confinement pressures are applied hydraulically and the sample is compressed axially. Figure 2.3 shows the schematic of a typical triaxial test setup used to in soil testing. Triaxial tests are limited to low confinement pressures, typically on the order of 10 MPa. High confinement pressures are difficult and expensive due to, a) the design of hydraulic chamber to withstand high pressures, b) the design of flexible membrane jacketing the test specimen to withstand percolation of the hydraulic fluid at high pressures. Triaxial tests also do not prevent barreling deformations in the specimen. Hence, triaxial tests at high pressures are difficult to conduct and hence the results are rare.

An easier and less expensive method of reaching high confinement stresses is achieved by the method of confined compression. Ma and Ravi-Chandar [21] developed a method of characterizing the complete stress-strain behavior of materials using the configuration of confined compression. Figure 3.1 shows a schematic of the confined compression technique. The material to be tested is mounted in a hollow metallic cylinder called the confinement, and compressed axially using cylindrical pins. The metallic cylinder provides confining pressures to the sample. The presence of the confining cylinder also prevents inhomogeneous deformations in the sample, thereby relieving concerns of buckling, bulging and shear banding.The axial stresses are measured using a load cell mounted on the test frame. Axial strains are measured using an extensometer. The elastic response of the cylinder to the radial expansion of the sample

is measured by a strain gage mounted on the outer surface of the confinement. This strain gage measures the hoop strain on the outer surface of the confinement. The measured hoop strain is used to determine the radial pressure acting on the sample using the Lamé solution for plane stress, as the cylinder is free to expand axially, shown in Eqn. (3.1).

$$\sigma_{rr} = \sigma_{\theta\theta} = \frac{(b/a)^2 - 1}{2} E_c \epsilon_h \tag{3.1}$$

E_c is the modulus of the confinement and ϵ_h is the measured hoop strain. The stress and strain states of the sample in the confinement are given in the Section 3.2.

Ma and Ravichandar [21] demonstrated the method of confined compression on an aluminum alloy (Al 6061-T6). Using a confinement made of hardened AISI 4340 steel, a cylindrical sample made from aluminum was tested. Figure 3.2 shows the variation of axial stress with axial strain. The initial rise portion is the elastic region followed by yielding and unloading regions in the curve. The modulus obtained from the slope of initial rise in the curve was found to be 71 GPa, corresponding to the Young's modulus of aluminum. Yielding was found to occur at 280 MPa, which is in agreement with the yield strength of aluminum. The initial rise changes into a horizontal line, indicating yielding of aluminum sample. Poisson's ratio measured from the plot of hoop strain versus axial strain, in Figure 3.3, gives an initial value of 0.3. The hoop strain increased quickly

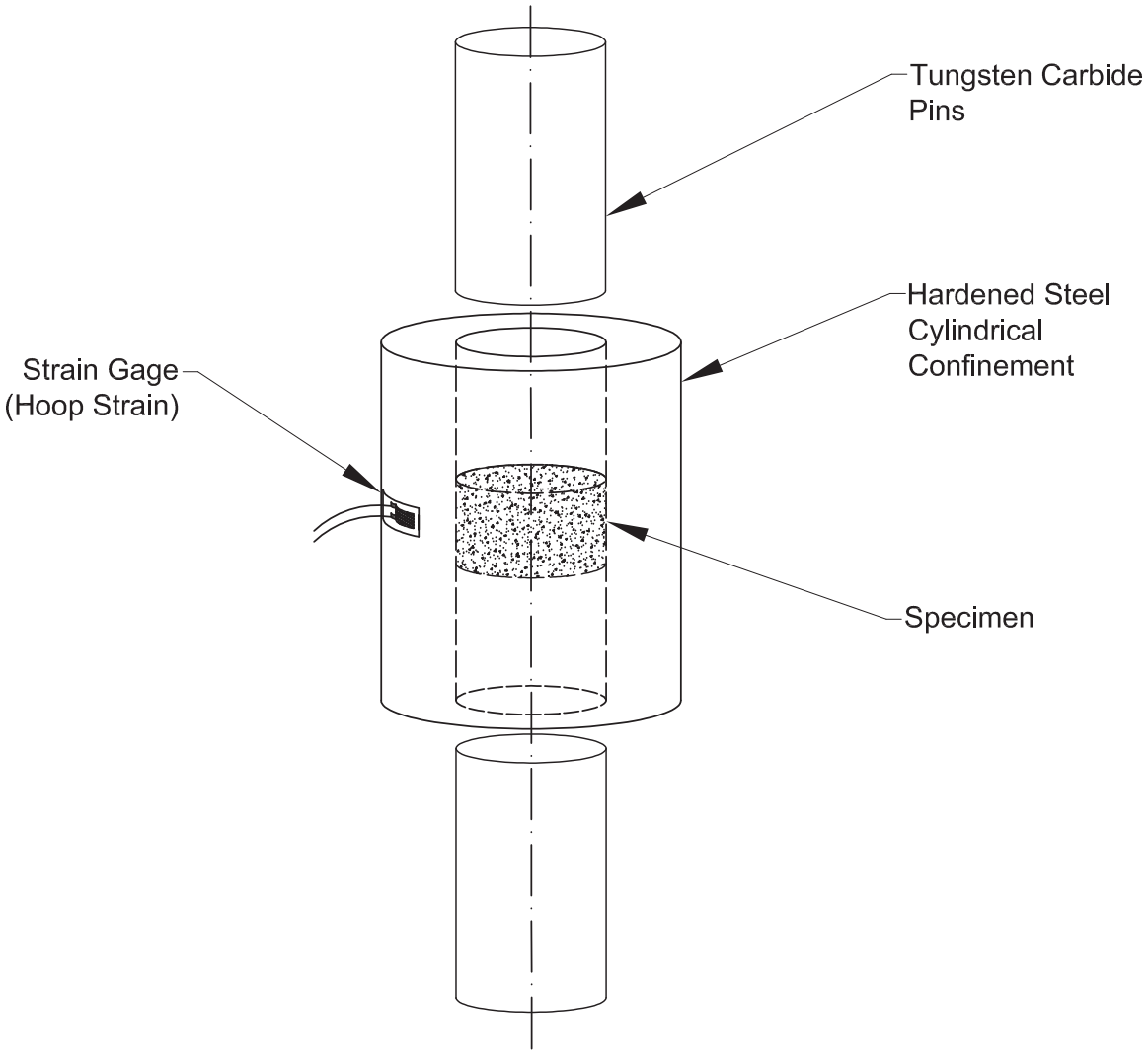

Figure 3.1: Schematic of confined compression setup showing the location of the specimen in the cylindrical confinement with tungsten carbide pins and strain gages.

after yielding had occurred due to plastic incompressibility.

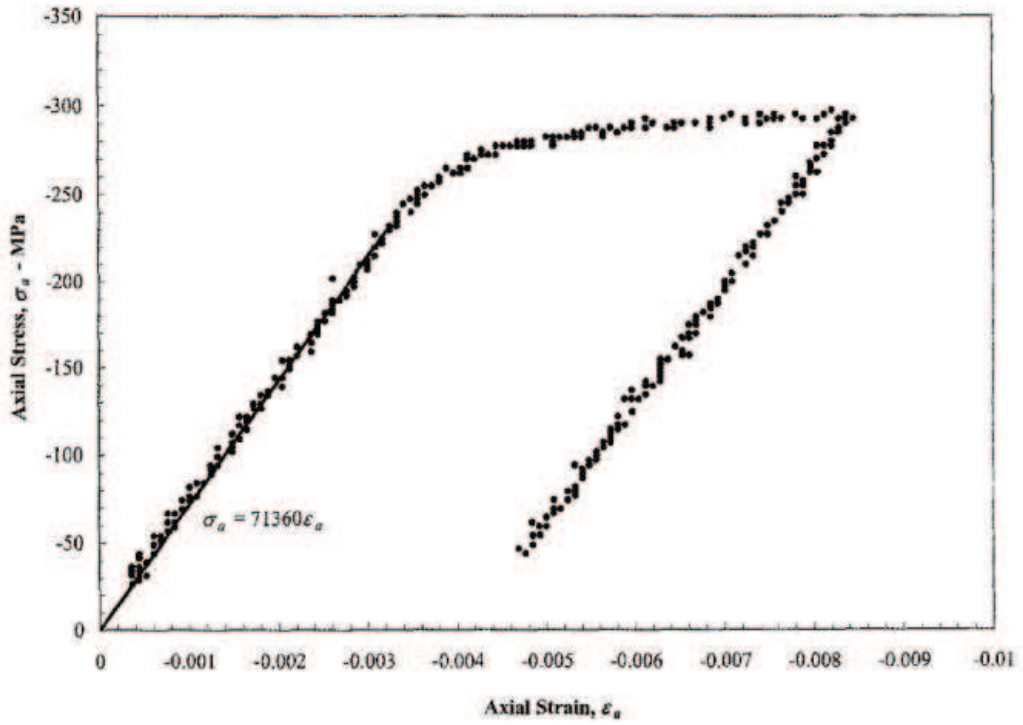

Figure 3.2: Plots of axial stress versus axial strain for confined compression tests on aluminum (Al 6061-T6) alloy. (after Ma and Ravichandar [21])

The bulk modulus of aluminum was calculated from the elastic slope of the mean stress versus volume dilatation plot, as shown in Figure 3.4. The value of bulk modulus was found to be 57.5 GPa. The three elastic constants, namely, Young's modulus, poisson's ratio, and bulk modulus of aluminum were determined from a single test using the method of confined compression. This technique has also been successfully applied to characterize polymers [25], ceramics [9], borosilicate glass [8] and concrete [11].

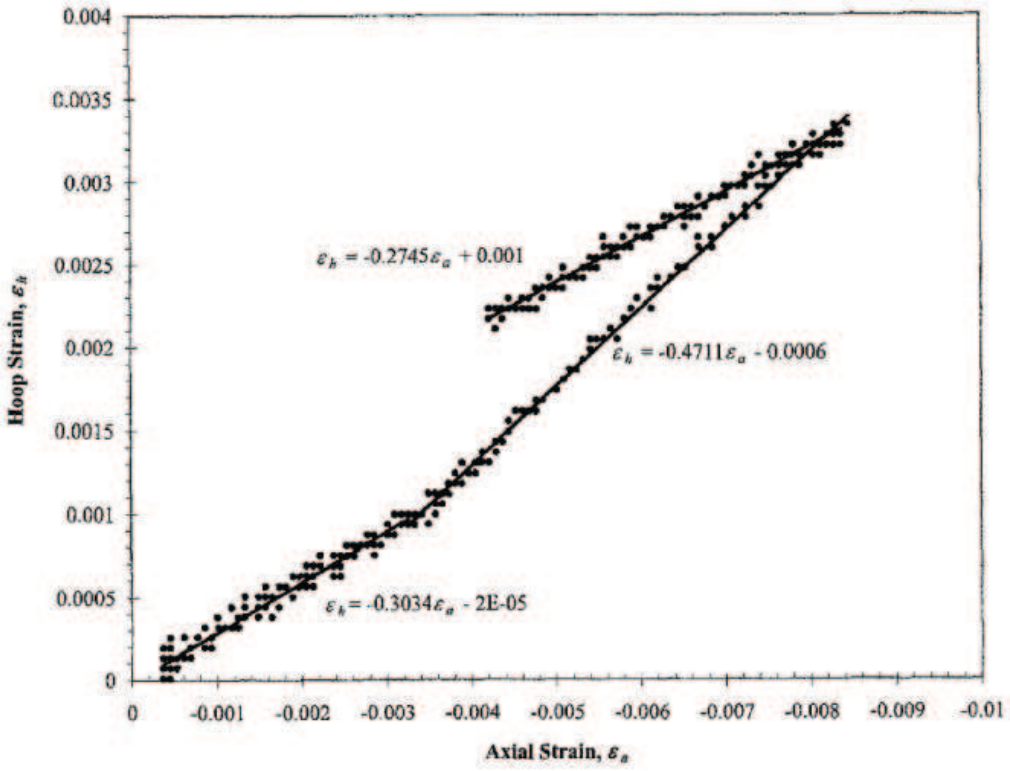

Figure 3.3: Plots of hoop strain versus axial strain for confined compression tests on aluminum (Al 6061-T6) alloy. (after Ma and Ravichandar [21])

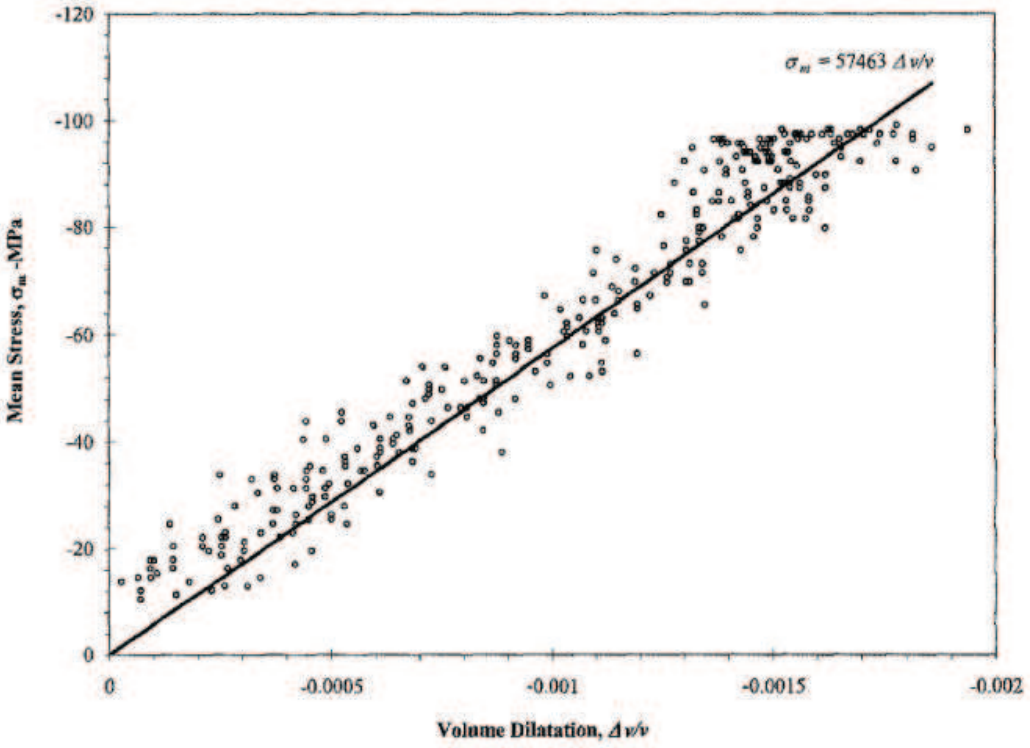

Figure 3.4: Plots of mean stress versus volume dilatation, for confined compression tests on aluminum (Al 6061-T6) alloy. (after Ma and Ravichandar [21])

3.2 Stress Analysis of the Confined Specimen

The test specimen in the confined compression technique has a cylindrical geometry with a diameter of '2a'. The confinement has an outer diameter of '2b' and an inner diameter of '2a'. The specimen is carefully machined to prevent any loss of contact between the inner surface of the confinement with the outer surface of the sample. A very tight tolerance clearance close to zero is needed so that the expansion of the sample and the confinement is continuous from the start of the test. The confinement is designed such that it remains elastic throughout the test and exhibits compliance that is measurable by the hoop strain gage. The elastic condition of the confinement is to prevent the complexity in stress analysis stemming from the plastic deformation of the sleeve. Hanina *et al.* [15] and Rittel *et al.* [26] demonstrated the use of confinement beyond the elastic limit, to maintain constant confining pressure. By varying the thickness of the confinement, different confining pressures were obtained.

The axial pressure (σ_{zz}) is obtained from the force measured by the load cell mounted in the axial direction. The axial strain (ϵ_{zz}) in the sample is obtained from the extensometer mounted on the cylindrical pins. The hoop strain (ϵ_h) is obtained from the strain gage mounted on the confinement.

The state of stress and strain is obtained from the theory of elasticity [29] in the confined specimen in cylindrical coordinate system is obtained from Eqn. (3.2). The equations are valid for confinement within its elastic

range and the contact between the confinement and the test specimen is frictionless [21, 25]. E_c and ν_c are the Young's modulus and Poisson's ratio of the confinement. Thus, the three measured quantities provide a complete description of the stress and strain components of the material under evaluation.

$$\sigma_{rr} = \sigma_{\theta\theta} = \frac{(b/a)^2 - 1}{2} E_c \epsilon_h \tag{3.2}$$

$$\sigma_{zz} = \sigma_a \tag{3.3}$$

$$\epsilon_{rr} = \epsilon_{\theta\theta} = \frac{\epsilon_h}{2}\left[(1-\nu_c) + (1+\nu_c)\frac{b^2}{a^2}\right] \tag{3.4}$$

$$\epsilon_{zz} = \epsilon_a \tag{3.5}$$

The principle stress and strain components from Eqn. (3.2) are used to derive the dilatational and deviatoric components. The hydrostatic stress and strain components are given in Eqn. (3.6).

$$\text{Mean stress}, \sigma_m = \frac{\sigma_{zz} + 2\sigma_{rr}}{3} \tag{3.6}$$

$$\text{Volume dilatation}, v = \epsilon_{zz} + 2\epsilon_{rr} \tag{3.7}$$

The deviatoric components of stress and strain components are given by

Eqn.(3.8).

$$s_{zz} = \frac{2}{3}(\sigma_{zz} - \sigma_{rr}) \tag{3.8}$$

$$s_{rr} = s_{\theta\theta} = -\frac{1}{3}(\sigma_{zz} - \sigma_{rr}) \tag{3.9}$$

$$s_{max} = \tau_e = \frac{1}{2}(\sigma_{zz} - \sigma_{rr}) \tag{3.10}$$

$$\epsilon_{zz} = \frac{2}{3}(\epsilon_{zz} - \epsilon_{rr}) \tag{3.11}$$

$$\epsilon_{rr} = \epsilon_{\theta\theta} = -\frac{1}{3}(\epsilon_{zz} - \epsilon_{rr}) \tag{3.12}$$

The maximim shear stress and shear strain are given by Eqn.(3.13)

$$\tau_e = \frac{1}{2}(\sigma_{zz} - \sigma_{rr}) \tag{3.13}$$

$$\gamma_e = (\epsilon_{zz} - \epsilon_{rr}) \tag{3.14}$$

Void ratio

$$e = \frac{\rho_s(1 + \epsilon_z z)}{\rho_0} - 1$$

CHAPTER 4

PROBLEM STATEMENT

The response of sand to high pressures has been actively investigated for military and civil applications. Penetration of projectiles in sand, barriers to withstand from explosions, deep water drilling for oil extraction and mining are some applications concerned with the behavior of sand at high pressures. At this time, no constitutive model for predicting the behavior of sand at a wide range of pressures is available. Factors such as grain shape, size, strength, and moisture content contribute to the complexity of the model. Processes such as grain interactions and grain fracture also need to be included in the development of the model. Experimental characterization of the mechanical behavior of sand under compression is essential to the development and verification of such a constitutive model.

Based on the literature review, presented in the previous two chapters, it can be seen that even though the mechanical behavior of sand has been investigated for almost a century, much of it has been under pressures below 100 MPa. For pressures above 100 MPa, the investigations have

been somewhat limited. One of reasons for this limitation has been the lack of experimental facilities to reach higher stresses. Studies in the field of geotechnical engineering have concentrated on low pressures, as high stresses (above 100 MPa) are rather uncommon, such as in sand embankments, building foundations, and structures on sand. The need for extending the investigations to higher pressures have been expressed by various researchers [2, 13, 22, 31, 32]. Fracture and compaction of the fractured powders have been found to occur at high pressures. The extension of results obtained from low pressure studies might not be valid at high pressures. This can be noted from the results reported by Hagerty *et al.* [13] where sands of different shapes, sizes, and mineralogies eventually approached a common 'moduli' in the stress-strain curves. The effect of moisture on the stress-strain behavior of sand has been unclear. While Hendron [17] reported a rise in the slope of stress-strain curves, Martin *et al.* [23] observed a decrease in the slope when compared to dry sand. Traditional approach for characterization of the behavior of sand using triaxial testing has shown limitation in the attainable stresses on sand. Recently developed technique of confined compression to characterize metals, brittle materials such as glass, and polymers has been used . The relative simplicity of this technique and its ability to reach higher confinement pressures overcomes the limitations of triaxial testing in the characterization of materials.

This experimental investigation aims to characterize the behavior of

Eglin sand at axial pressures of up to 3 GPa which has not been reported in the literature. Confinement pressure of up to 800 MPa has not been reported either. A review of the literature shows that investigations up to axial stresses of 850 MPa. Using the technique of confined compression, the mechanical behavior of sand under uniaxial compression is investigated in this thesis. The primary factors considered are initial density, particle size, and moisture content. Four different densities of sand are investigated, namely, 1.55, 1.60, 1.65, 1.70 g/cm^3. The effect of particle size on the mechanical behavior is investigated at two sizes, namely, 0.850-0.600 mm size range and 0.212-0.150 mm. The effect of moisture on the stress-strain behavior of sand is investigated at 0%, 5%, 10%, and 20% of water by weight. A test fixture has been designed and built to reach high axial pressures of 3 GPa and axial strains of 30%. The axial and radial stress-strain data obtained from the experiments are used to derive the hydrostatic and shear stress states. The results of this investigation are presented in this study.

CHAPTER 5

EXPERIMENTAL METHODS

This chapter presents details on the experimental methodology of confined compression tests on sand. The description of the compression fixture, method of sample preparation, test conditions, data acquisition and analysis are covered in this chapter.

5.1 Self-Aligning Compression Fixture

A self-aligning compression fixture was designed and fabricated in-house to conduct high pressure tests on Eglin sand. The fixture assembly consists of a top steel platen, hollow steel enclosure, steel ball, steel confinement, and two tungsten carbide rods/pins. Figure 5.1 shows a schematic of the fixture. The criteria for the design of the fixture are a) to reach high axial stresses of 3 GPa in the sand sample, b) to prevent non-uniform stresses along the cross-section of the sand sample arising from rotation of the sample while testing and misalignments in the test frame, c) to measure displacements independent of the system compliance, and d) to place the

confined sample at the same location between the platens for each test to maintain repeatability.

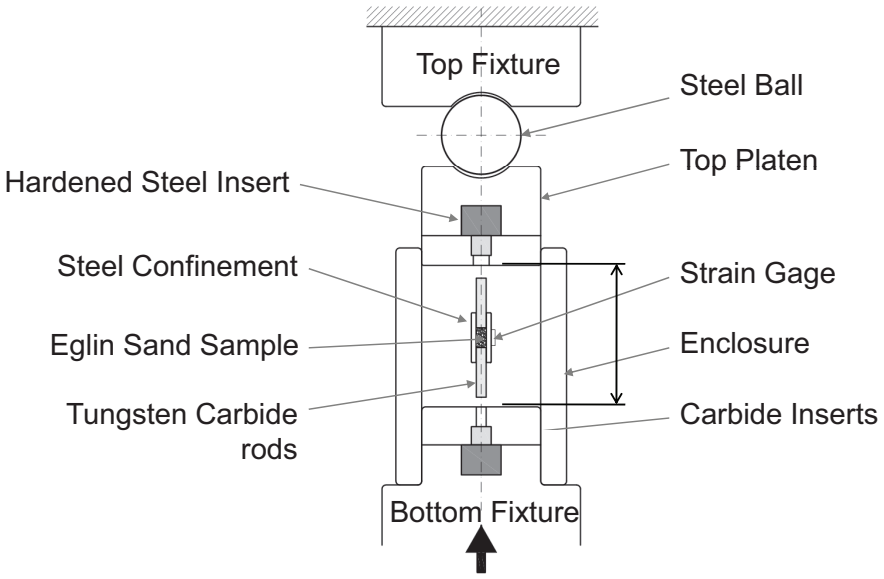

Figure 5.1: Schematic of self-aligning static compression fixture

Tests were carried out on an MTS servo-hydraulic uniaxial testing machine equipped with a 245 kN (55,078 lbf) MTS load cell and Instron Fastrack 8800D controller. The maximum achievable load on this frame was limited to 180 kN (40,465 lbf). With restrictions in the loading range, the sample diameter was fixed at 6.35 mm (0.25 in.) to achieve axial stress of 3 GPa at 100 KN load. The sample was confined in a metal sleeve made of A2 tool steel with internal diameter of 6.35 mm (0.25 in.). The loading

platens were designed with two steps stress reducers. A 0.50 in. diameter tungsten carbide (WC) insert followed by a 1 in. diameter hardened D2 tool steel (hardness of HRC 62) insert was press fitted in the top and bottom platens to prevent yielding from axial and contact stresses, as shown in Figure 5.4. The top and bottom platens were made of AISI 4340 steel. Sand was confined in hardened A2 tool steel confinement with outer diameter of 12.70 mm (0.50 in.) and inner diameter of 6.35 mm (0.25 in.).

The confinement was bored from 12.70 mm (0.50 in.) A2 tool steel rod to an internal diameter of 6.34 mm ($0.25^{+0.0005}_{-0.0000}$ in.). The length of the confinement was 25.4 mm (1.0 in.). It was heat-treated in an oven to a temperature of 1100$\pm$10°C and air-quenched. Tempering was performed at 180$\pm$10°C to relieve stresses and to increase toughness. Rockwell hardness measurements made after heat treatment showed an average hardness of HRC 58 on the outer curvature of the confinement. After heat treatment, the inner bore was re-finished with a 120 grit (Silicon carbide) flex-hone tool at 1200 rpm for 60 seconds. A smooth bore is necessary to minimize friction between the inner walls of the confinement and the sand sample. Measurement of friction between the sand particles and the walls of the confinement was not possible. In order to reduce the effect of friction, the length of the sand sample was kept small, the value being 8 mm for the least dense samples.

Tungsten carbide rods were used to compress the sample in the

confinement. The WC rods had a diameter of 6.34 mm ($0.25^{+0.0000}_{-0.0005}$ in.) and a length of 31.75 mm (1.25 in.). To accommodate for the expansion of the WC rods in the confinement during the tests, the WC rods were smaller than the bore diameter of the confinement. The WC rods were cut from a longer stock rod using a diamond saw at a machine shop. The WC rods had 10% cobalt content (binder) with submicron grain size. This grade of WC rods have an estimated hardness of HRA 92, modulus of elasticity of 580 GPa and compressive strength of 5.5 GPa (based on the information provided by the manufacturer, Kennametal Inc.). The high strength, smooth surface finish and hardness of WC, make it an ideal choice of material for compression of sand to high pressures. The rods exhibited resistance to indentation and wear by sand grains even after numerous rounds of tests.

5.2 Test Instrumentation

A strain gage was mounted on the exterior surface of the confinement to measure the hoop strains. Vishay WK-13-125BZ-10C bonded strain gage with a grid resistance of 1000 Ω, a gage factor of 2.08, a gage length of 3.18 mm (0.125 in.), and a grid width of 1.57 mm (0.062 in.) was used. Narrow gage width and gage length are important to reduce the averaging of strain signals at the measured area. High resistance gage provides increased sensitivity and better signal to noise ratio. The high endurance lead wires in this gage contributes to its high fatigue life. The

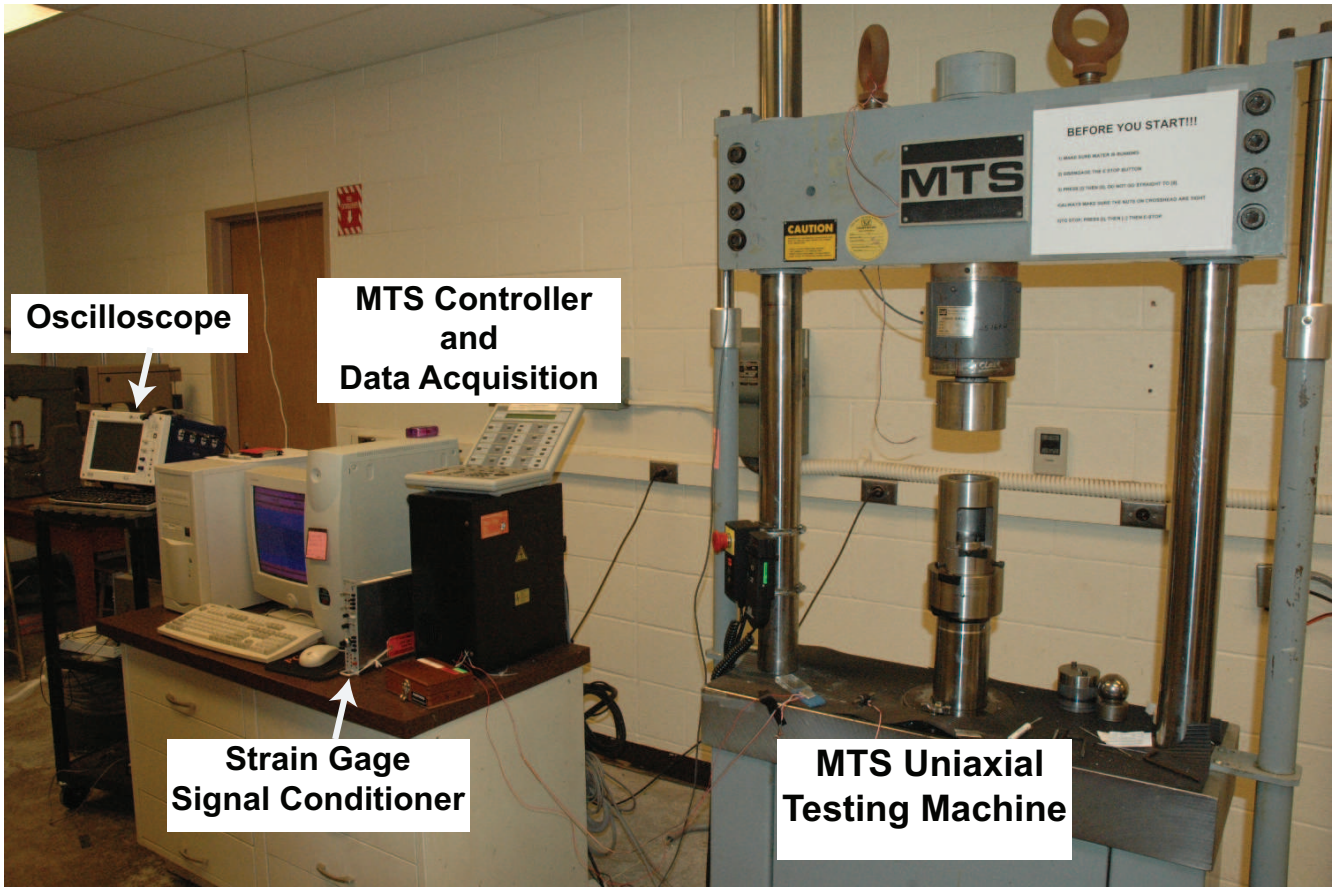

Figure 5.2: A photograph of the quasi-static test setup for the mechanical testing of sand. It shows the load frame, test fixture, controls, and data acquisition and signal conditioning equipment.

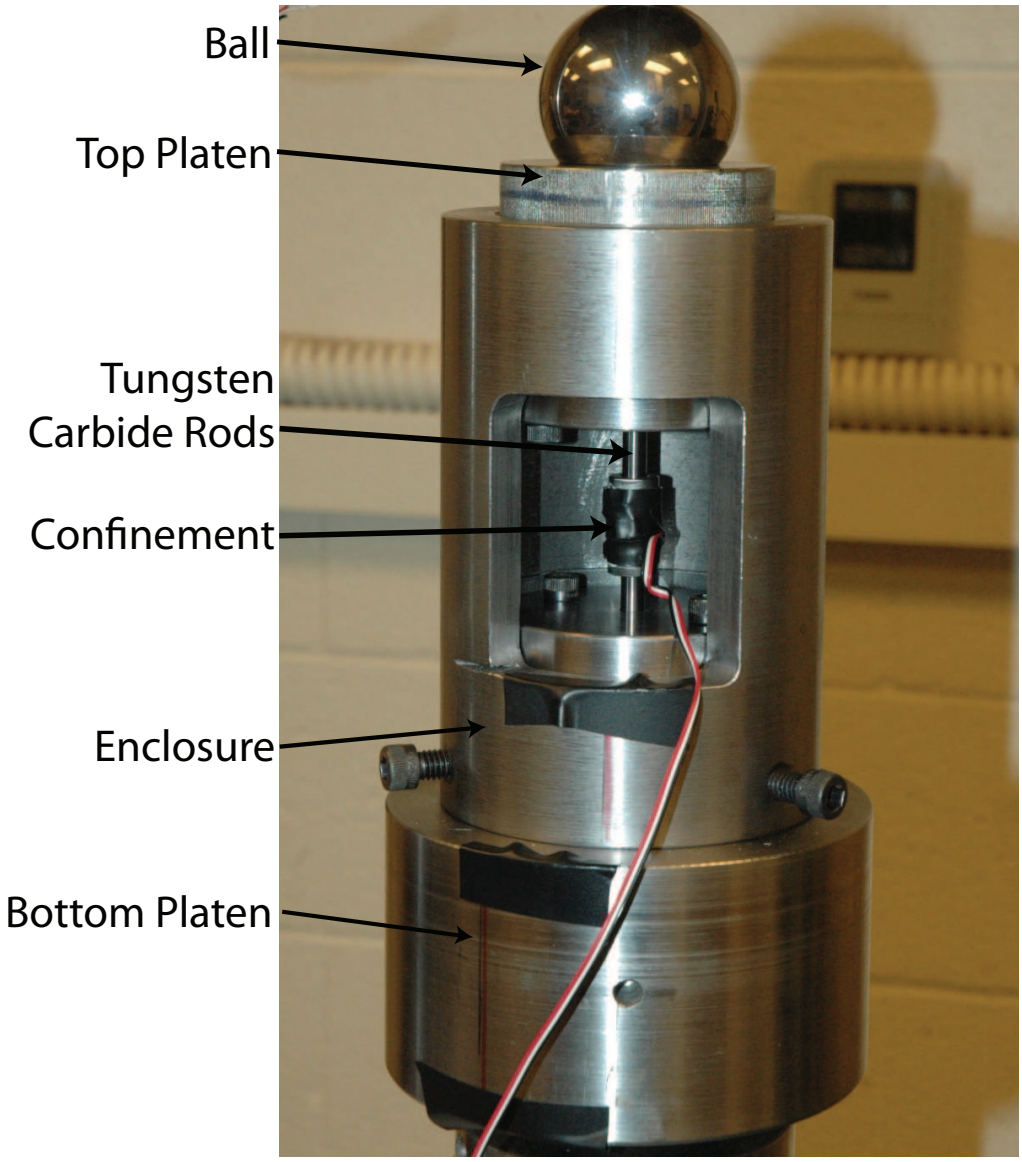

Figure 5.3: A photograph of the self-aligning static compression fixture, showing the confinement and loading pins located in the bottom platen, inside the enclosure with the top platen.

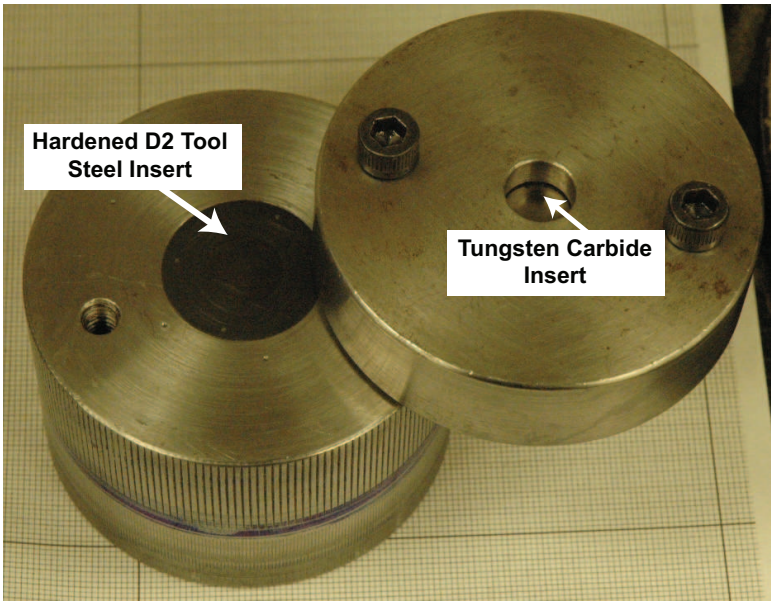

Figure 5.4: A photograph of the disassembled top platen showing the two tungsten carbide inserts and hardened D2 tool steel inserts. The inserts are sequentially placed to relieve the contact stresses between the tungsten carbide loading pins and the steel platen.

strain gage was connected to three other inactive resistors to complete a full Wheatstone bridge. The leads from the Wheatstone bridge were connected to Vishay 2310A signal conditioner and amplifier. The 2310A provided strain gage measurement capabilities, namely, bridge excitation, bridge balancing, shunt calibration, amplification and signal filtering. 15 V bridge excitation was chosen for maximum source amplification of the measured signal without introducing thermal drift in the measured signals from the strain gage. The tests were performed at room temperature of 22°C. Due to the static nature of testing, a low pass filter of 10 Hz was chosen to reduce the influence of electromagnetic interferences on the the measured signal. A gain of 100 was chosen for amplifying the measured signals as

it provided a good signal to noise ratio. Prior to testing, the 2310A is switched on for approximately 20 minutes to attain a 'steady-state'. The analog output (0-10 V) of the signal conditioner was then connected to a Nicolet Sigma-30 oscilloscope which digitized (12-bit resolution) and sampled at 50 Hz. Signals from the Instron controller and the Nicolet oscilloscope were synchronized. The measured strain gage response (V_m in Volts) was converted to equivalent strain (ϵ_h) using Eqn. (5.1), where 'GF' is the gage factor of the strain gage, 'V_{ex}' is the excitation voltage in Volts and 'G' is the amplifier gain.

$$\epsilon_h = \frac{4 \times V_m}{GF \times V_{ex} \times G} \tag{5.1}$$

5.3 Eglin Sand - Particle Size Analysis

The sand used in this study was received from the Eglin Air Force base (Eglin AFB), Florida. Particle size analysis was conducted on the Eglin sand based on ASTM D2487 standard [1]. The procedure for particle size analysis involves screening sand through a series of stacked sieves of decreasing mesh size. Eleven sieves, each 3 inch in diameter (manufactured by Dual Mfg. Co.) based on ASTM E-11 specifications, were used in this analysis. Sieve sizes of 14, 18, 20, 30, 35, 40, 50, 70, 100, 140, and 270 were used in the particle size analysis. 100 grams of sand was taken and poured on the largest sieve and the whole assembly of stacked sieves were shaken for about 20 minutes using a mechanical shaker (Dual Mfg. Co.,

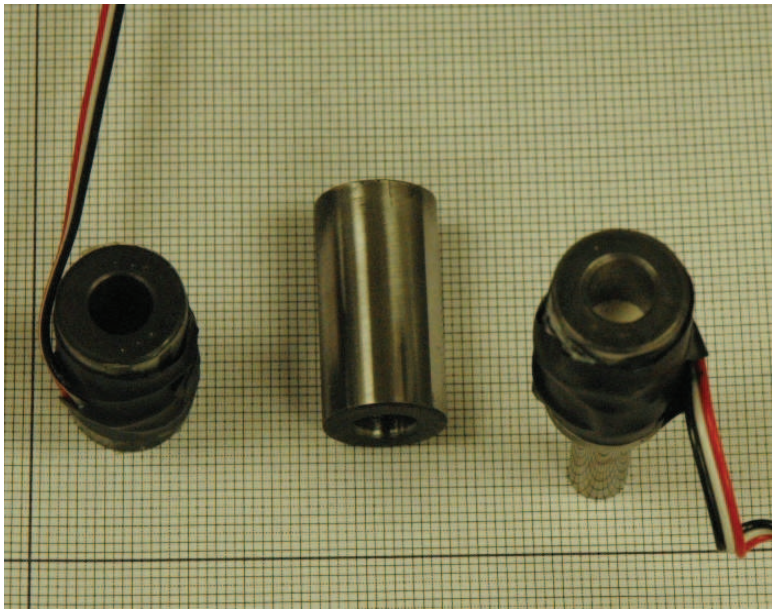

Figure 5.5: Photograph of the confinements used in the static testing of sand. The confinement (to the left) has a bonded strain gage mounted under the protective tape. The confinement (to the right) shows the compacted sand sample after test routine. The confinement (in the middle) shows a polished surface for mounting strain gage.

Model # D-4326) shown in Figure 5.6. Table 5.1 gives the values recorded from the particle size analyzer. The cumulative plot of % mass of sand passed through each sieve is plotted against the corresponding sieve size. The plot of grain size distribution for Eglin sand is shown in Figure 5.7. The values of D_{10} and D_{60} are obtained from the grain size distribution plot. D_{10} and D_{60} are the diameters of sand grains for which 10% and 60% of the particles are finer, respectively. The co-efficient of uniformity, $C_U = \frac{D_{60}}{D_{10}}$, was calculated. C_U value of less than 4 indicates uniform particle size, as is the case with Eglin sand. Poorly graded sands have a steep size distribution curve. Based on Unified Soil Classification system (USCS),

Eglin sand is categorized as SP-SM. The symbol 'S' represents Sand, 'SP-SM' refers to poorly graded sand with silt. Table 5.2 summarizes the physical properties of Eglin sand obtained from sieve analysis and from previous literature survey [31].

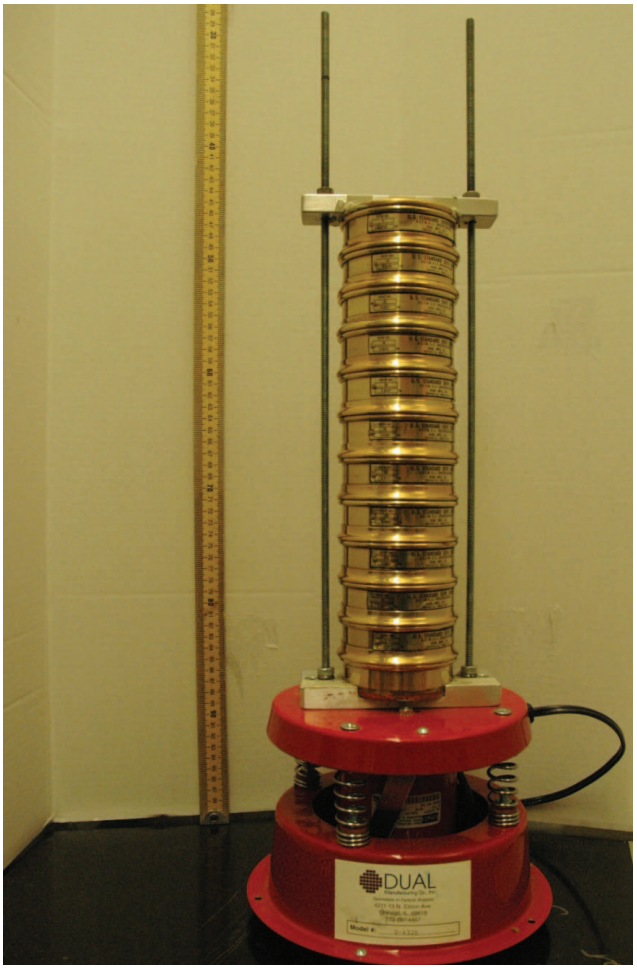

Figure 5.6: A photograph of the mechanical shaker used in the particle size analysis.

Table 5.1: Particle size analysis of Eglin sand. The values recorded below are obtained from the sand gradation tests conducted.

Sieve#	Sieve opening (mm)	Mass of sand collected (g)	Mass of sand passed (g)	Percentage finer
14	1.400	0.087	99.913	99.91
18	1.000	0.044	99.870	99.87
20	0.850	0.075	99.795	99.79
30	0.600	8.873	90.922	90.92
35	0.500	13.430	77.492	77.49
40	0.425	16.852	60.640	60.64
50	0.300	29.956	30.684	30.68
70	0.212	18.374	12.310	12.31
100	0.150	6.623	5.687	5.69
140	0.106	3.313	2.374	2.37
270	0.053	1.456	0.918	0.92
Pan		0.231	0	0.00

Table 5.2: Physical Properties of Eglin sand

USCS Classification	SP-SM
Specific Gravity	2.65 (reported by [31])
D_{50} or Average grain size	0.375 mm
D_{60} Particle Size	0.420 mm
D_{10} Particle Size	0.197 mm
Uniformity, $C_U = \frac{D_{60}}{D_{10}}$	2.13

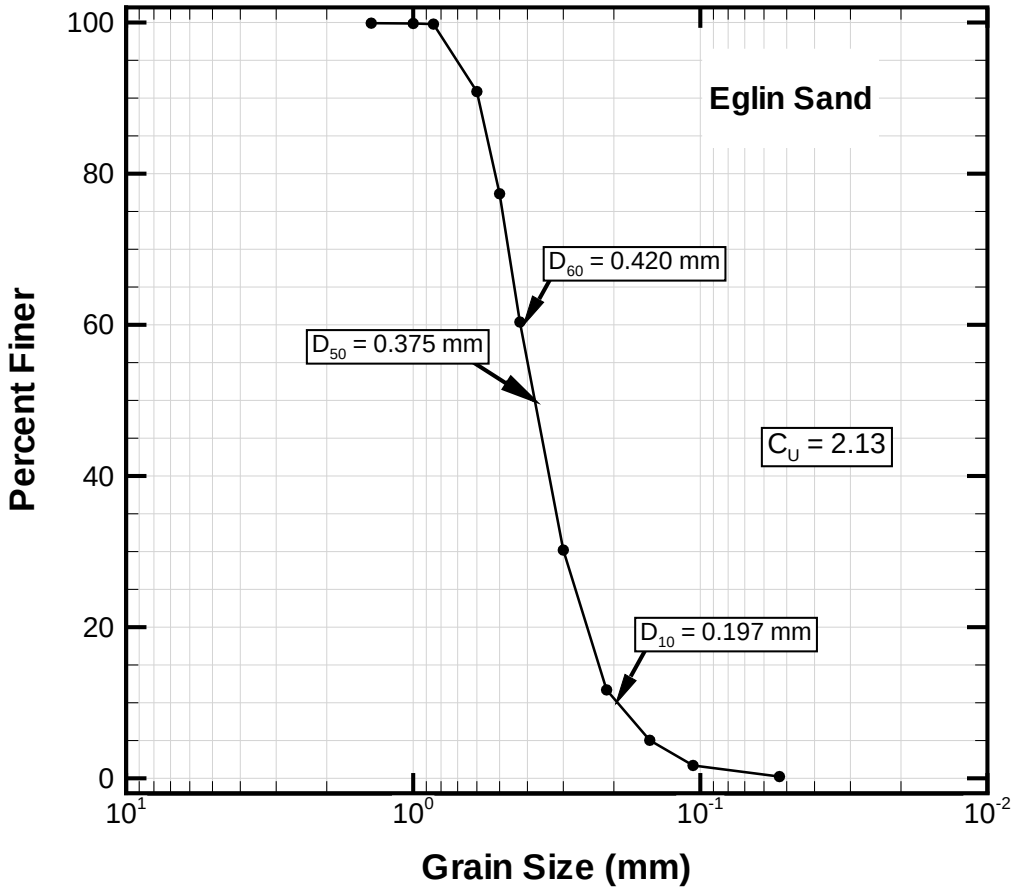

Figure 5.7: Sieve analysis for determining particle size distribution of Eglin sand. The steep curve indicates a poorly graded sand.

5.4 Sample Preparation

0.4±0.0004 grams of sand was weighed using a balance (Denver Instruments APX-200 with 0.1 mg resolution) and poured into the confinement with the bottom WC rod in place. Care was taken to prevent loss of sand grains during the transfer. The top WC rod was inserted into the

confinement and the assembly was compacted. Since no standard methods for compaction exist, the assembly was gripped firmly in hand and gently tapped on a rubber pad. The assembly was rotated after every few taps to prevent the settling of smaller sand grains. This was done to maintain the heterogeneous distribution of sand grains. The length of the rods was measured from time to time to check if the sand specimen was compacted to the desired density based on Eqn. (5.2).

$$\rho = \frac{m}{\frac{\pi}{4} d^2 \left(L_{measured} - L_{solidlength}\right)} \tag{5.2}$$

5.4.1 Tests on the effect of initial density

Four densities of sand, namely, 1.55, 1.60, 1.65, and 1.70 g/cm^3 were chosen to investigate the effect of initial packing density on the mechanical behavior of Eglin sand. Table 5.3 lists the length of sand sample corresponding to different initial densities. Care was taken to ensure that the sample was placed in the mid-length of the confinement to ensure accurate measurement of the hoop stresses by the strain gage mounted on the confinement. The assembly was carefully placed in the compression fixture. The strain gage mounted on the confinement was then connected to the oscilloscope.

5.4.2 Tests on the effect of particle size

In the tests conducted to investigate the effect of particle size on the mechanical behavior of Eglin sand, coarse and fine particle sizes were

Table 5.3: Values of initial density and the corresponding lengths of sand sample.

Initial density (g/cm^3)	Length of sand (mm)
1.55	8.21
1.60	7.96
1.65	7.72
1.70	7.49

chosen. The coarse samples consisted of sand passing sieve 20 and collected at sieve 30 (denoted by '20-30'). The fine samples consisted of sand passing sieve 100 and collected at sieve 140 (denoted by '100-140'). The Eglin sand is primarily contains particles between sieve 40 and 50 (denoted by '40-50'). The sand samples were compacted to a density of 1.55 g/cm^3.

5.4.3 Tests on the effect of moisture content

The effect of moisture content on the mechanical behavior of Eglin sand was investigated at four different degrees of saturation, namely, 0, 20, 40, and 100%. 100 grams of as-received Eglin sand was dried in an oven at 105°C for 3 hours. The mass of sand was measured before and after drying to determine the amount of moisture present in the as-received Eglin sand. The moisture content was estimated to be about 0.1% by weight. The effect of moisture was investigated at the initial density of 1.60 g/cm^3. Oven-dried sand was weighed and compacted as per the procedure described in page 54. The degree of saturation of water in the sand sample was

Table 5.4: Volume and degree of saturation of water in 1.60 g/cm^3 dry Eglin sand sample.

Volume of Water (μl)	Percentage Mass of Water (%)	Degree of Saturation (%)
20	5	20
40	10	40
100	25	100

controlled by injecting a pre-determined amount of distilled water using a 100 μl syringe (Gastight #1710, Hamilton Co., Reno, Nevada) with a blunt needle. The sand sample was compacted by gently tapping on the confinement to achieve a density of 1.60 g/cm^3 and uniform distribution of moisture. Table 5.4 shows the relationship between the volume of water and degree of water saturation in 0.4 g of dry Eglin sand.

5.5 Method of Testing

The tests were performed under constant displacement mode. The bottom fixture was gradually raised till a pre-loading of 0.040 kN was attained. This was done to maintain uniform strain of 50% (before compliance correction) for all tests. A ramp loading profile for the actuator was chosen. A displacement rate of 0.002 mm/s was selected. Figure 5.8 shows the profile of ramp loading used in the tests. This corresponds to a strain rate of 0.002 s^{-1}, which falls in the quasi-static test regime. The axial forces from the load cell and the crosshead displacements from the encoder mounted on the MTS frame are recorded by the DAQ connected to the Instron FastTrack controller at 50Hz sampling frequency.

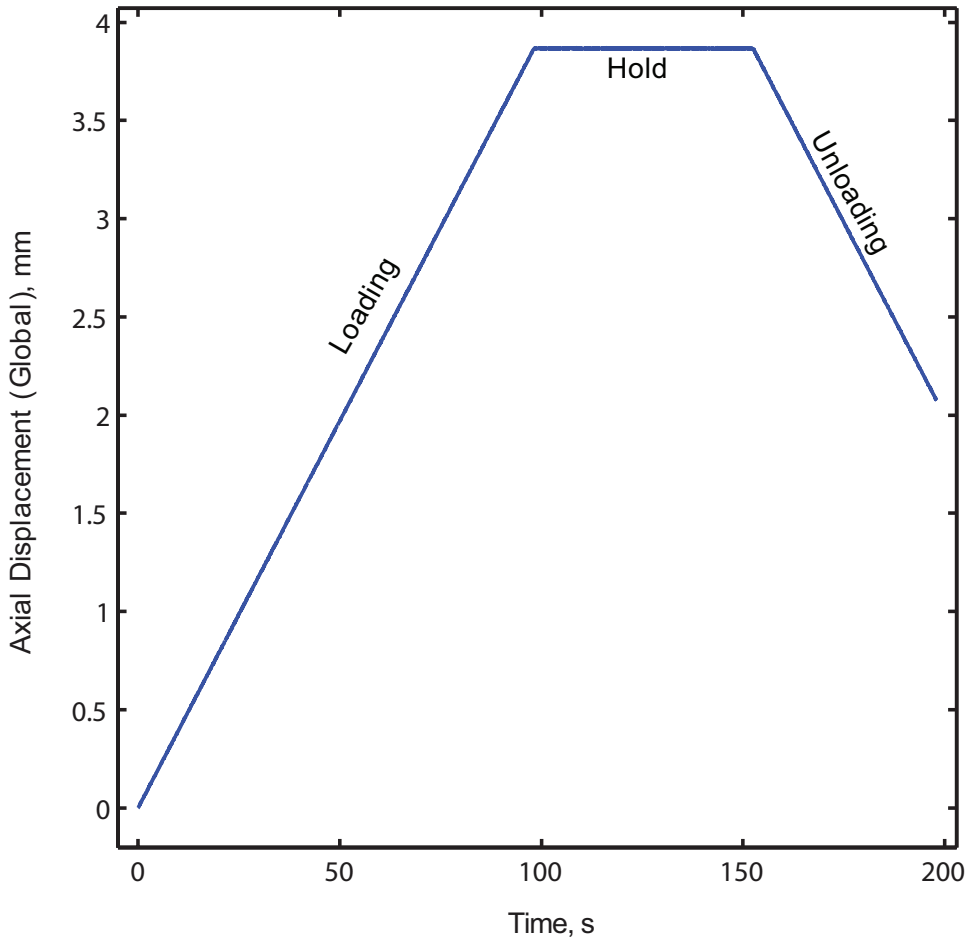

Figure 5.8: Loading and unloading profile showing constant displacement rate of 0.002 mm/s.

Upon completion of the test, the crushed sand in the confinement is collected. The bore of the confinement is cleaned with 91% isopropyl alcohol using a cotton tipped applicator to remove all the sand particles from the previous test leaving the confinement dry and clean for the next test. The confinements were used repeatedly for various tests until the indentation marks of the sand on the bore of the confinement were prevalently seen. Yielding in the confinement was not observed as the

output of the hoop strain gage showed repeatability in the sample tests done at the highest density of sand (1.70 g/cm^3) that was tested.

5.6 Characterization of Fixture Compliance

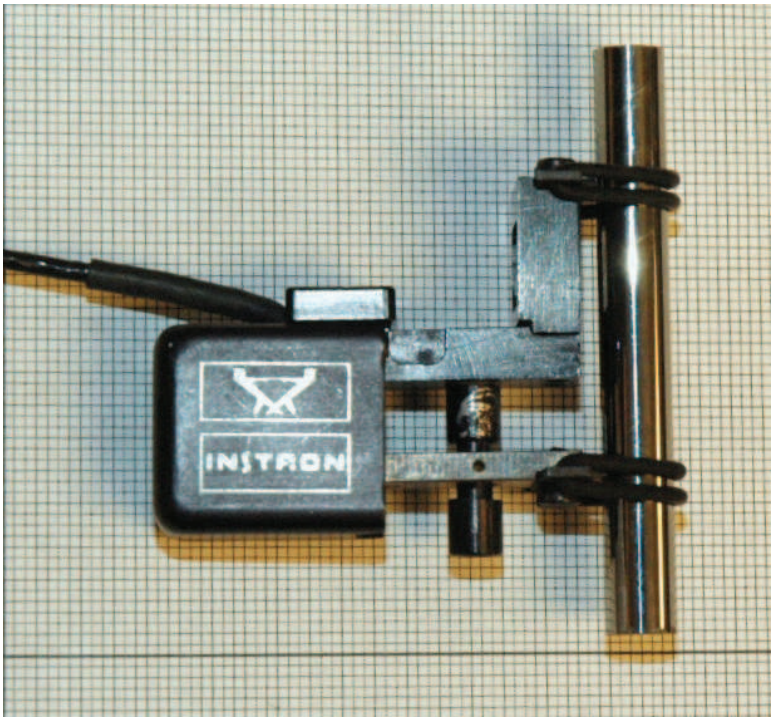

Figure 5.9: Photograph showing an extensometer attached to the tungsten carbide rod for machine compliance correction tests.

Measurement and characterization of the compliance of the load frame (including the test fixture) are necessary for precise determination of the specimen strains. Compliance in the system arises from deflection of individual components in the load frame which can be significant at high loads. In order to measure the true deformation of the sample, the deflections of the test frame at the same loads need to be subtracted.

Instron strain gage extensometer (catalog number 2620-828) with a gage length of 25.4 mm (1.00 in.) and a full-scale deflection of $\pm$1.27 mm ($\pm$0.05 in.) was mounted on the two WC rods to measure the displacement of the fixture without the sand sample, shown in Figure 5.9.

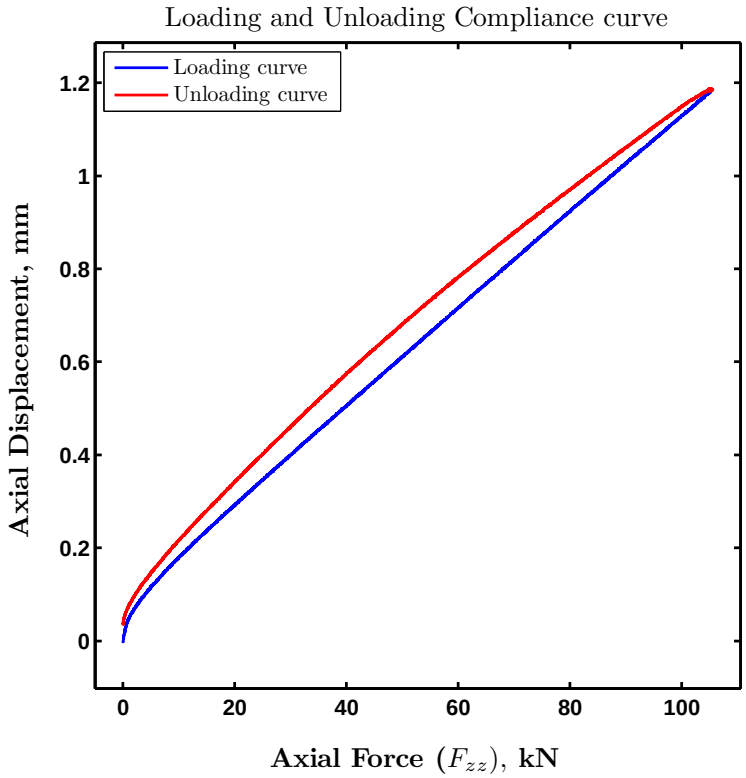

Figure 5.10: Load-displacement plot showing the compliance of the system without the sand sample.

The compliance tests were performed to a maximum load of 103 kN. Figure 5.10 shows the deflection in the system during loading and unloading of WC rods without the sand sample. The load-displacement curve shows an initial bend after which the loading curve remains linear.

The unloading curve exhibits hysteresis with a non-linear response. The presence of joints and contacts is considered to be the source of hysteresis in the loading-unloading paths. A 10^{th} order polynomial curve fitting was performed on the loading and unloading curves to obtain continuous polynomial functions for the loading and unloading cycles. The loading curve exhibited an initial bend after which it was linear, as can be seen in Figure 5.10. Ideally the loading and unloading curves of tests on sand can be corrected for compliance using the curve fits obtained from the compliance tests. However, in this study the loading curve was only used for compliance correction of both loading and unloading paths due to the difficulty in implementing the individual corrections. The existence of two displacement values at the points of transition from loading to unloading, showed discontinuity in the corrected plots of axial strains.

CHAPTER 6

RESULTS

Quasistatic uniaxial compression tests were conducted on Eglin sand to investigate the effect of (a) initial density, (b) particle size, and (c) moisture content. The uniaxial tests were performed on 0.4 g of (Eglin) sand in a hardened tool steel confinement fitted with a strain gage to measure the hoop strain in the confinement during quasi-static loading and unloading. Compliance correction was performed on all the measurements to obtain the strain in the sand specimen, as the measured displacement also included the compliance of the fixture. A constant strain rate of 0.002 s^{-1} was maintained during loading and unloading of sand samples. At least three tests were conducted for each parameter being investigated to ensure the repeatability of the measurements.

A Matlab code (refer Appendix B) was created to process the data collected from each test. The primary functions of this code were to read and synchronize the data from each channel, identify the beginning and the end of loading and unloading cycles, perform compliance correction,

determine the multiaxial stress-strain in the sand sample, and plot the processed data. Figure 6.1 shows the extent of synchronization in the axial and radial stress measurements in time. The radial stress is derived from the hoop strain measurement using elasticity theory as described by Equation (3.2).

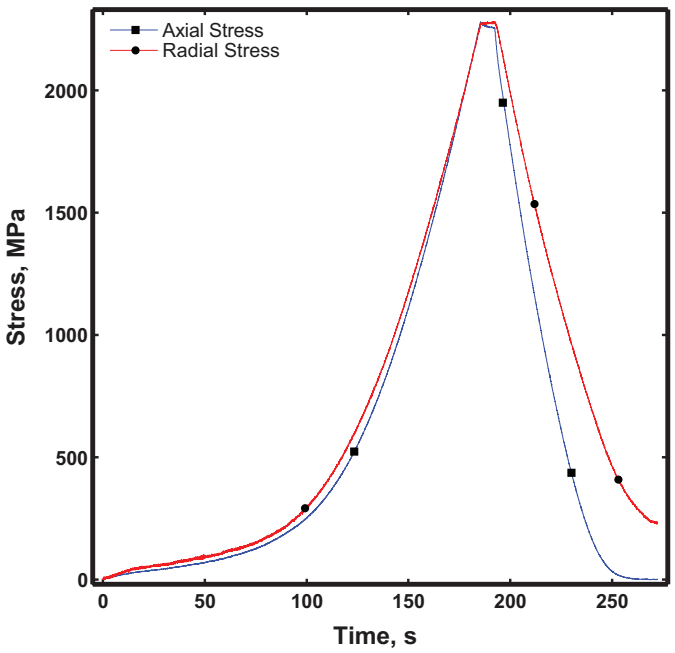

Figure 6.1: Plot demonstrating the synchronization of axial and radial stress measurements. The radial stress shown in this plot has been amplified to match the axial stress in order to demonstrate the extent of synchronization.

Sand samples were confined in hollow cylinders made from hardened A2 tool steel. Figure 6.2 shows the picture of dry, wet and crushed Eglin sand. The photograph shows dry Eglin sand to be yellow in color and the comminuted sand to be white in color. Sand was collected after each

test and separated using the sieve assembly in the mechanical shaker. Due to the small quantity (0.4 g) of sand being tested, accurate particle size distribution analysis was not possible. In all the dry tests, crushed sand particles were collected on the sieve 270 as well as the pan, after passing through sieves ranging from sizes 18 to 160. This shows that sand particles were completely crushed to fine sand and silt. Since Equations (3.2)-(3.5)

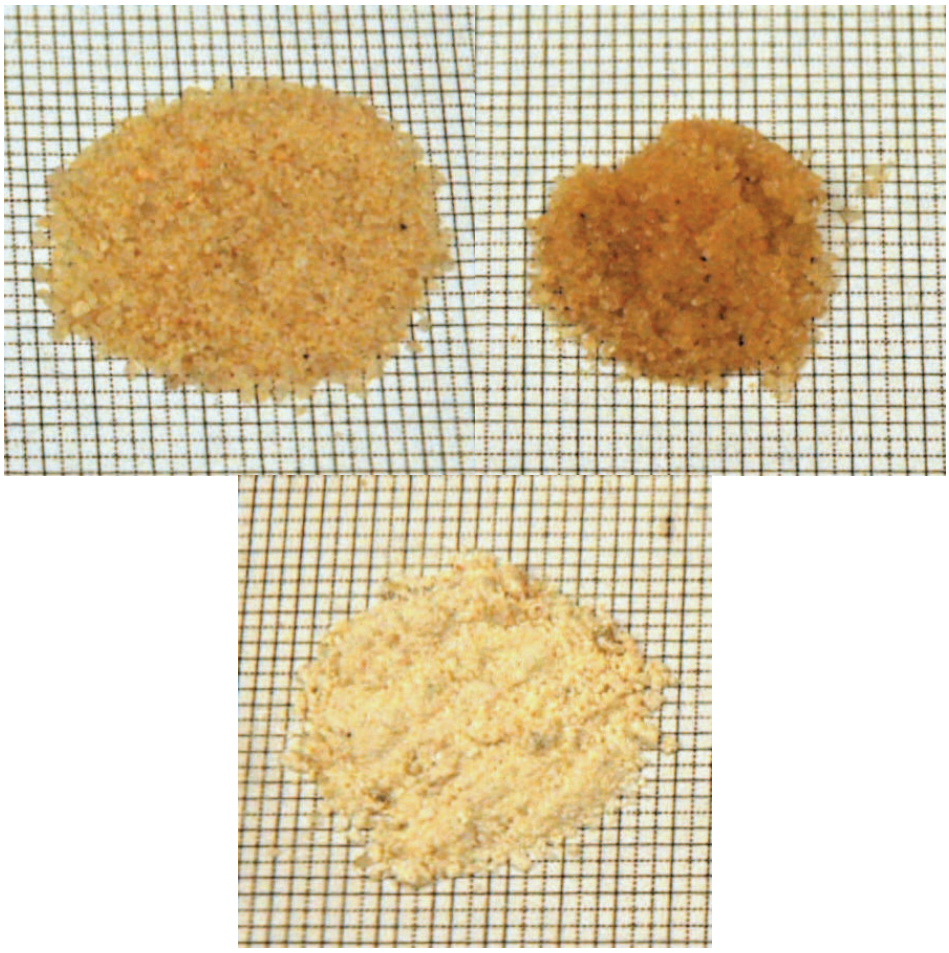

Figure 6.2: Samples of dry (to the top left) and wet (top right) Eglin sand before test. The bottom image shows the powdered sand sample after compression testing.

assume the confinement to undergo elastic deformation, it is necessary ensure that the confinement remains elastic during the test. Figure 6.3 shows the sectioned view of a confinement used in the testing of sand samples. The confinement shows bright discolorations due to exposure of the sand grains on inner surface of the confinement but no obvious signs of yielding otherwise. The repeatability of hoop measurements from multiple tests performed on the same confinement also show the absence of yielding in the confinement.

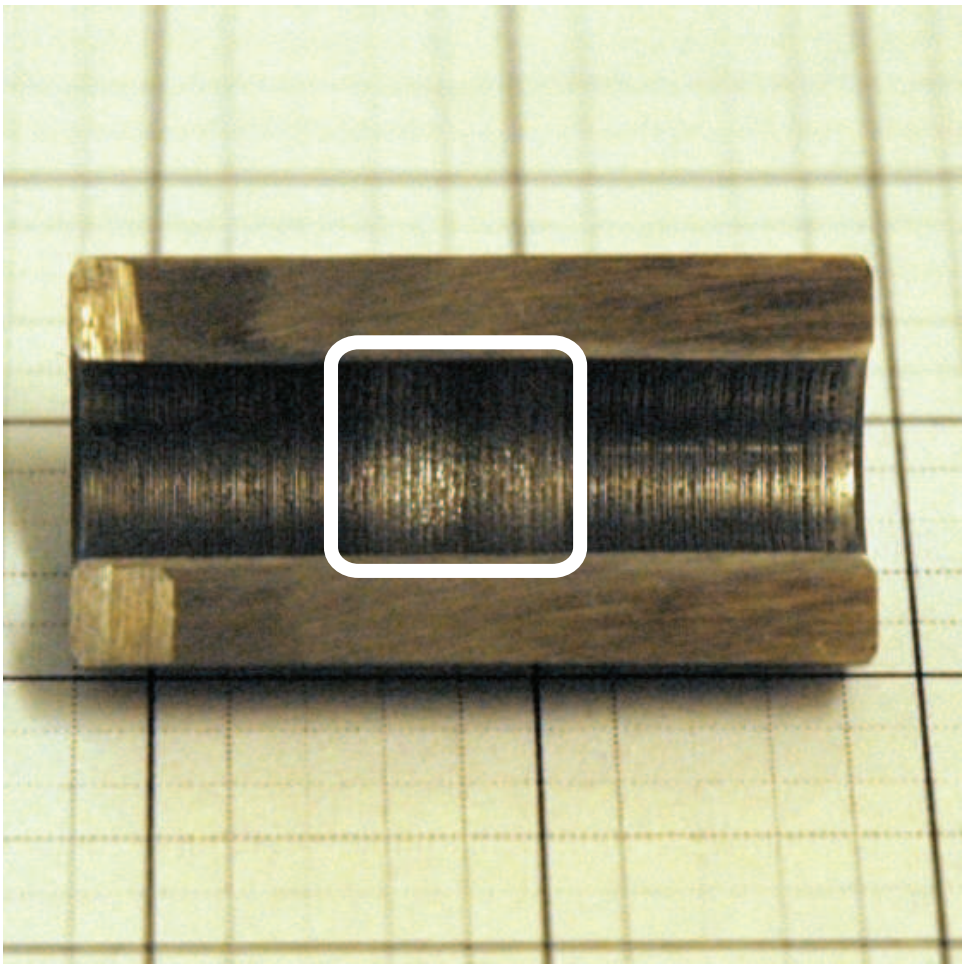

Figure 6.3: Cut-section view of confinement used in compression tests on sand samples showing intact (unyielded) surface.

Effect of initial density

Results of tests conducted to investigate the effect of initial density of dry sand on its mechanical behavior are presented in Figures 6.6 through 6.10. Minimum density of 1.55 g/cm^3 was attained by pouring the sand sample into the confinement and gently tapping it a few times to reach a sample length of 8.21 mm. Maximum density of 1.70 g/cm^3 was attained gently tapping the assembly for an extended period of time to reach a length of 7.49 mm. Three tests were conducted at each packing density for repeatability. Figures 6.4 and 6.5 show good repeatability in the axial stress-strain behavior for the lowest and highest initial densities. All experiments were conducted up to maximum axial strains of 35% after compliance correction. Axial strain of 35% was chosen based on the limitations of the test frame and the compression fixture. Tests conducted on the most dense configuration of sand, namely, 1.70 g/cm^3 reached maximum axial stress of 3.2 GPa at corresponding axial strain of 35%.

Four densities of Eglin sand, namely, 1.55, 1.60, 1.65, and 1.70 g/cm^3 were compressed to 35% axial strain at 0.002 s^{-1} strain rate. Figure 6.6 show the axial stress-strain plots. It is seen that the slope of the axial stress-strain curves increases as the initial density increases. Figure 6.7 show the plots of radial stress versus axial strain. As the initial density increases, the radial stress also increases. Figure 6.8 show the plots of hydrostatic

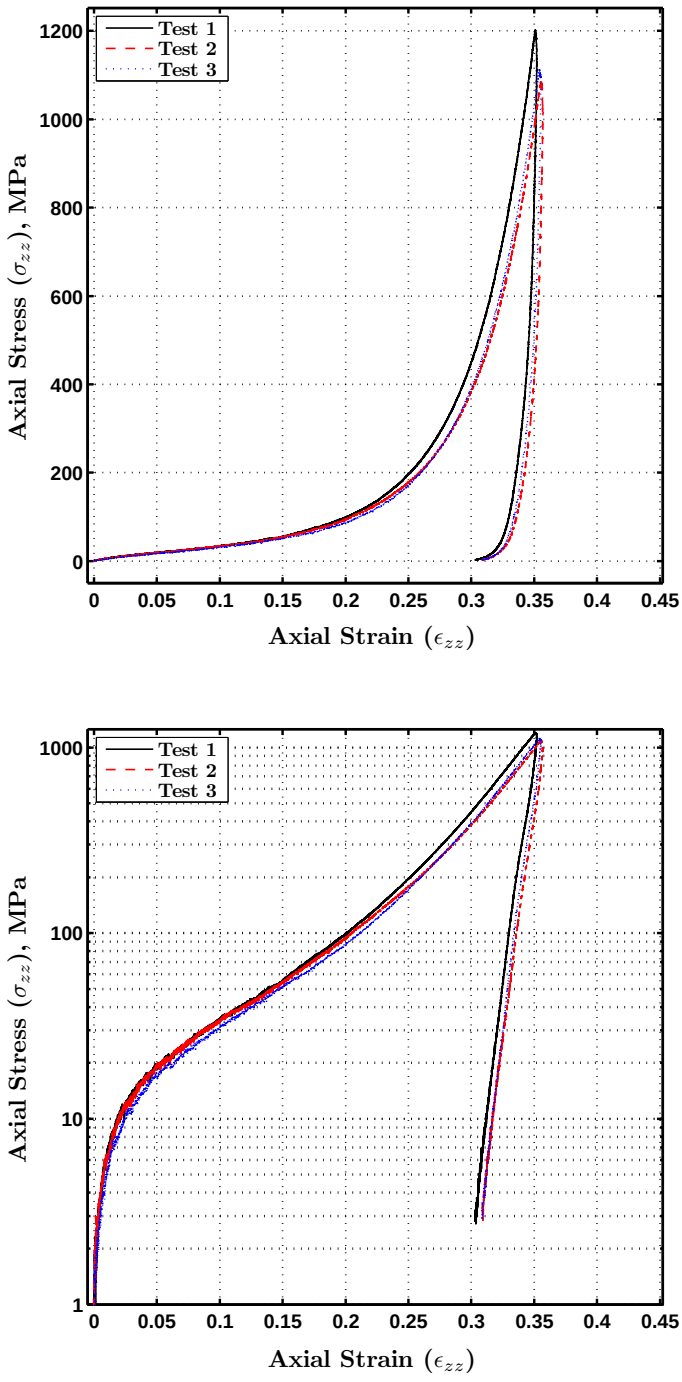

Figure 6.4: Linear and semi-log plot of axial stress vs axial strain from three trials conducted at low initial density of 1.55 g/cm^3 show experimental repeatability.

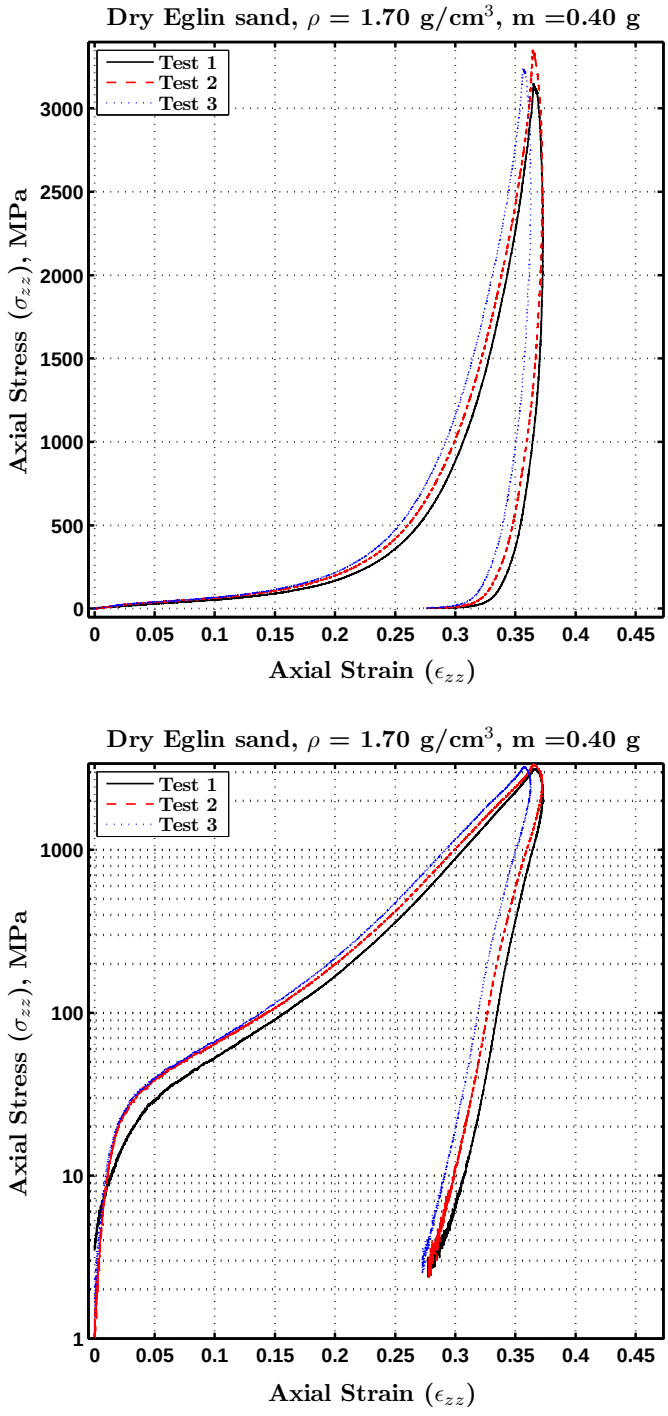

Figure 6.5: Linear and semi-log plot of axial stress vs axial strain from three trials conducted at high initial density of 1.70 g/cm^3 show experimental repeatability.

pressure versus volumetric strain. The hydrostatic stress increases with increase in initial density. The shear stress-strain plots are shown in Figure 6.9. The shear stress increases as the initial density increases. Figure 6.10 shows the semi-log plot of void ratio versus axial pressure. The semi-log plot shows the reduction of void ratio with increase in axial pressure.

Effect of particle size

Experiments were conducted on dry Eglin sand of two sizes, (a) passing sieve #20 but stopped by sieve #30 (20-30), and (b) passing sieve #70 but stopped by sieve #100 (70-100), to investigate effect of particle size on the mechanical behavior of sand. Poorly graded Eglin sand has a D_{50} value of 0.375 mm which corresponds to sieve sizes of 40-50. All tests were conducted at initial density of 1.55 g/cm^3. Figure 6.11 shows the axial stress-strain responses of sand particles. The smaller particles of 70-100, showed a stiffer response as compared to the larger particles of sieve size 20-30. The radial stress versus axial strain plots, shown in Figure 6.12, exhibit similar trend of increasing slope with decrease in particle size.

Effect of moisture content

The role of moisture on the mechanical behavior of sand was investigated. Oven-dried Eglin sand was injected with measured quantity of distilled water to attain desired degree of water saturation. Four different degrees

of saturation of water were tested. 0% (dry), 20%, 40%, and 100% (fully saturated) degrees of saturation were tested at the initial density of 1.60 g/cm^3. Figures 6.15, 6.16, 6.17, and 6.18 show the plots of axial, radial, hydrostatic, and shear stress-strain respectively. The plots show no difference in behavior of sand with change in degree of water saturation.

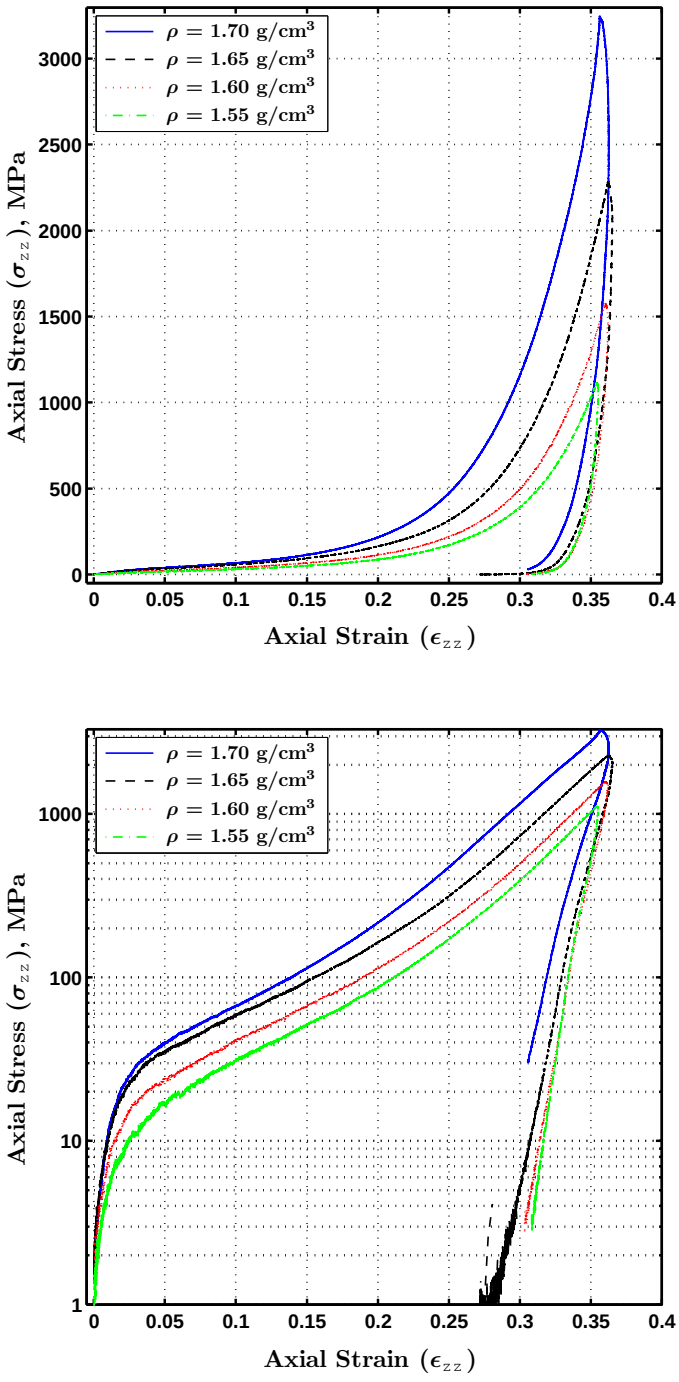

Figure 6.6: Linear and semi-log plot of axial stress vs axial strain for 1.55, 1.60, 1.65, and 1.70 g/cm^3 show increase in stiffness with increase in initial density.

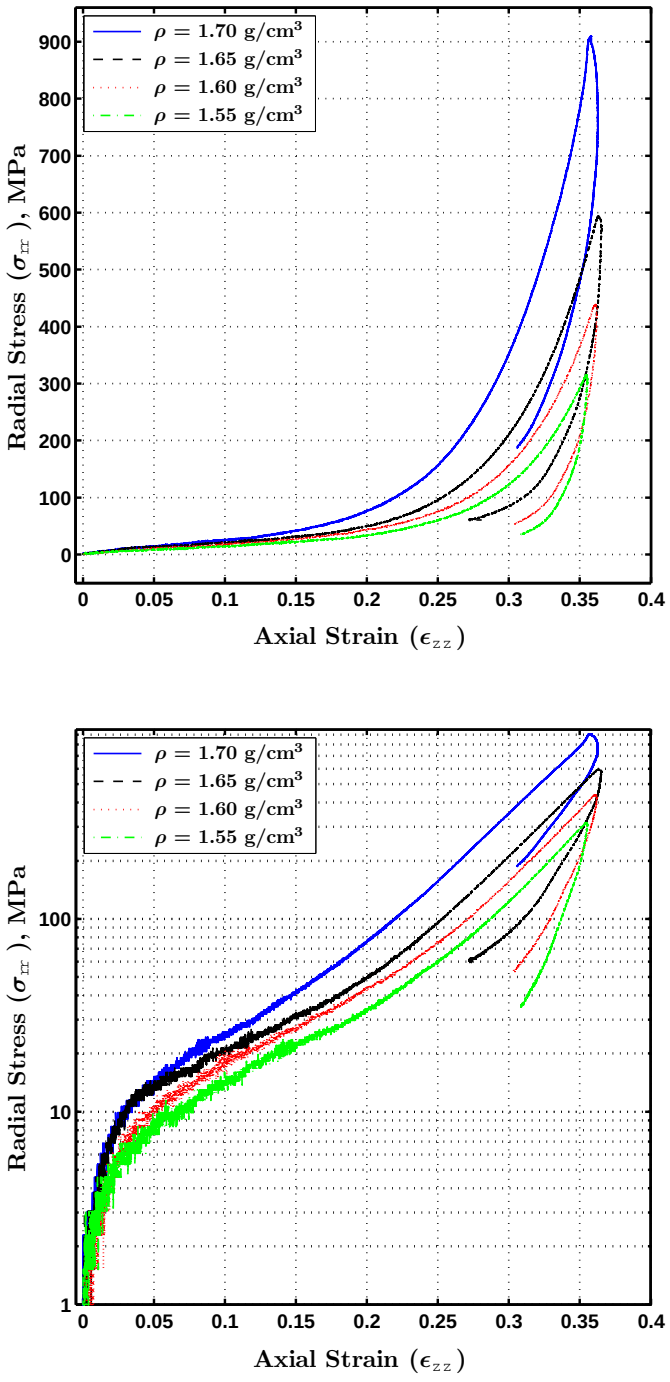

Figure 6.7: Linear and semi-log plot of radial stress vs axial strain for 1.55, 1.60, 1.65, and 1.70 g/cm^3 show increase in stiffness with increase in initial packing density.

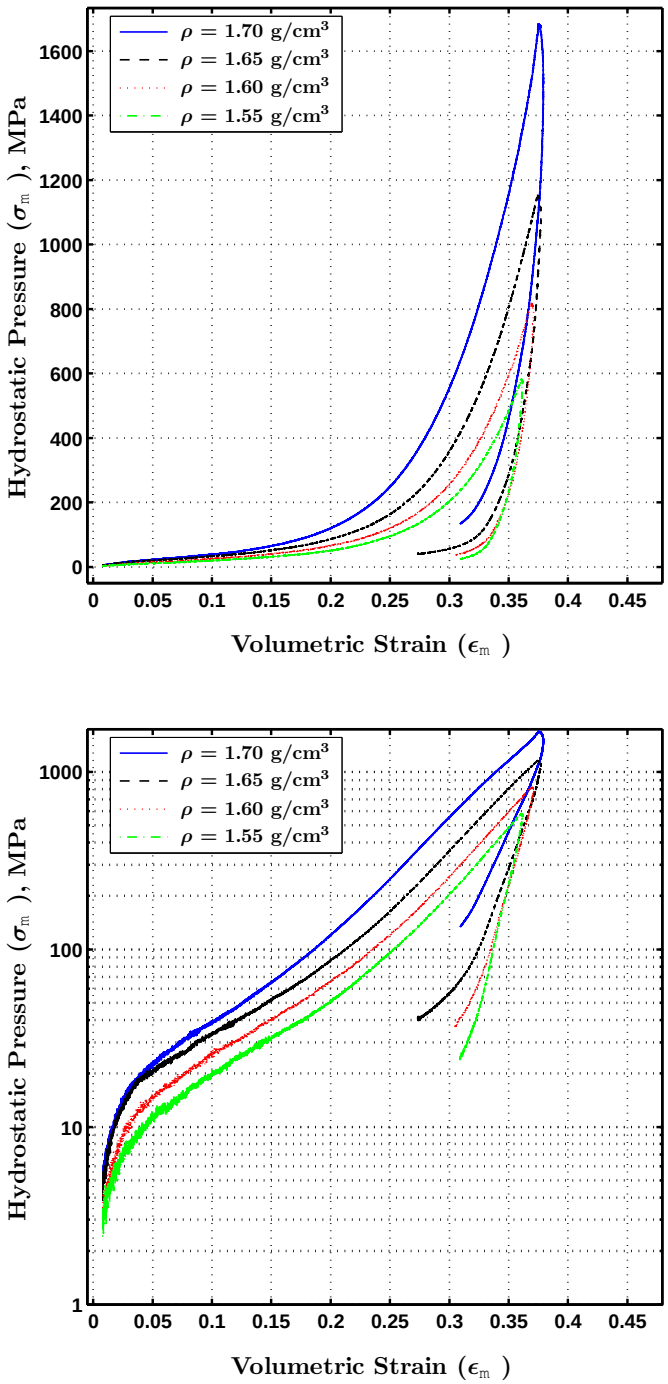

Figure 6.8: Linear and semi-log plot of hydrostatic pressure vs volumetric strain for 1.55, 1.60, 1.65, and 1.70 g/cm^3 show increase in stiffness with increase in initial packing density.

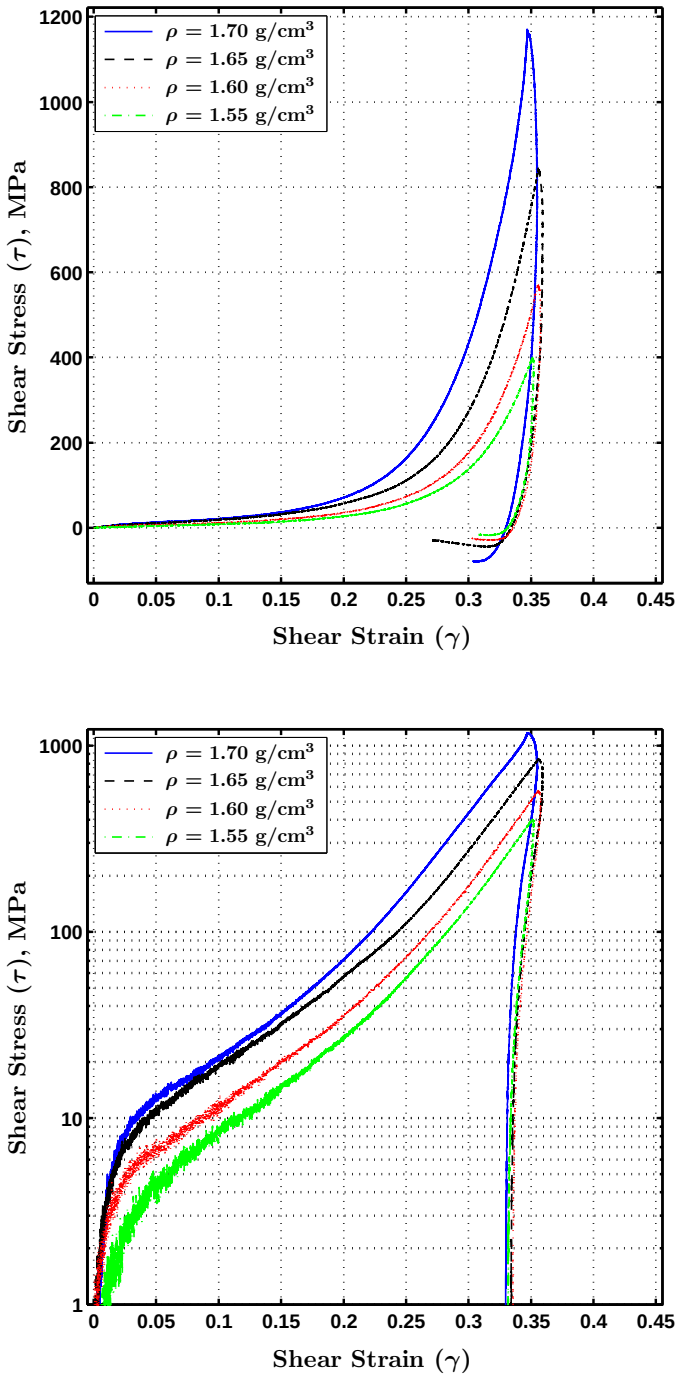

Figure 6.9: Linear and semi-log plot of shear stress vs shear strain for 1.55, 1.60, 1.65, and 1.70 g/cm^3 show increase in stiffness with increase in initial packing density.

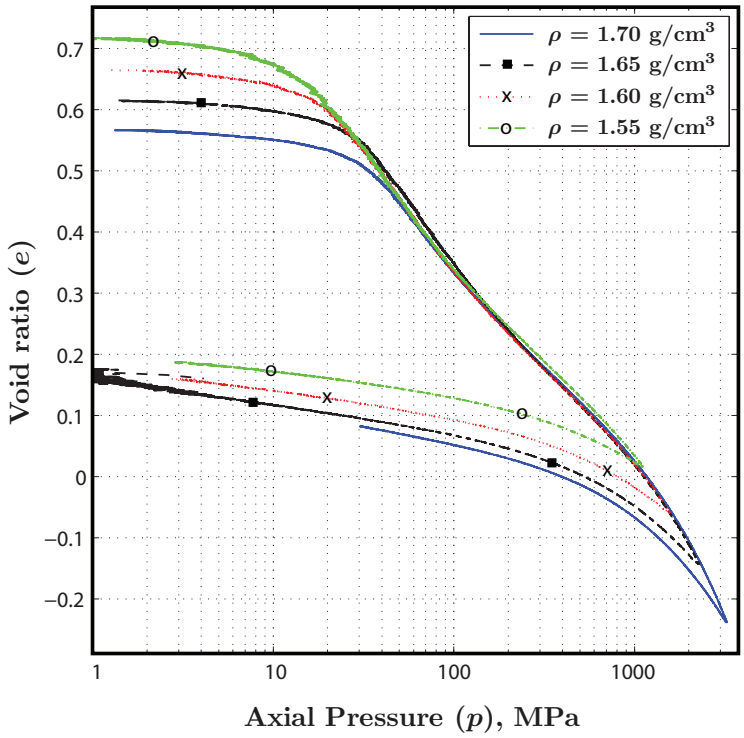

Figure 6.10: Semi-log plot of void ratio versus axial stress for 1.55, 1.60, 1.65, and 1.70 g/cm^3 show the unification of curves below $e = 0.5$. Negative void ratios are seen at axial pressures beyond 1 GPa.

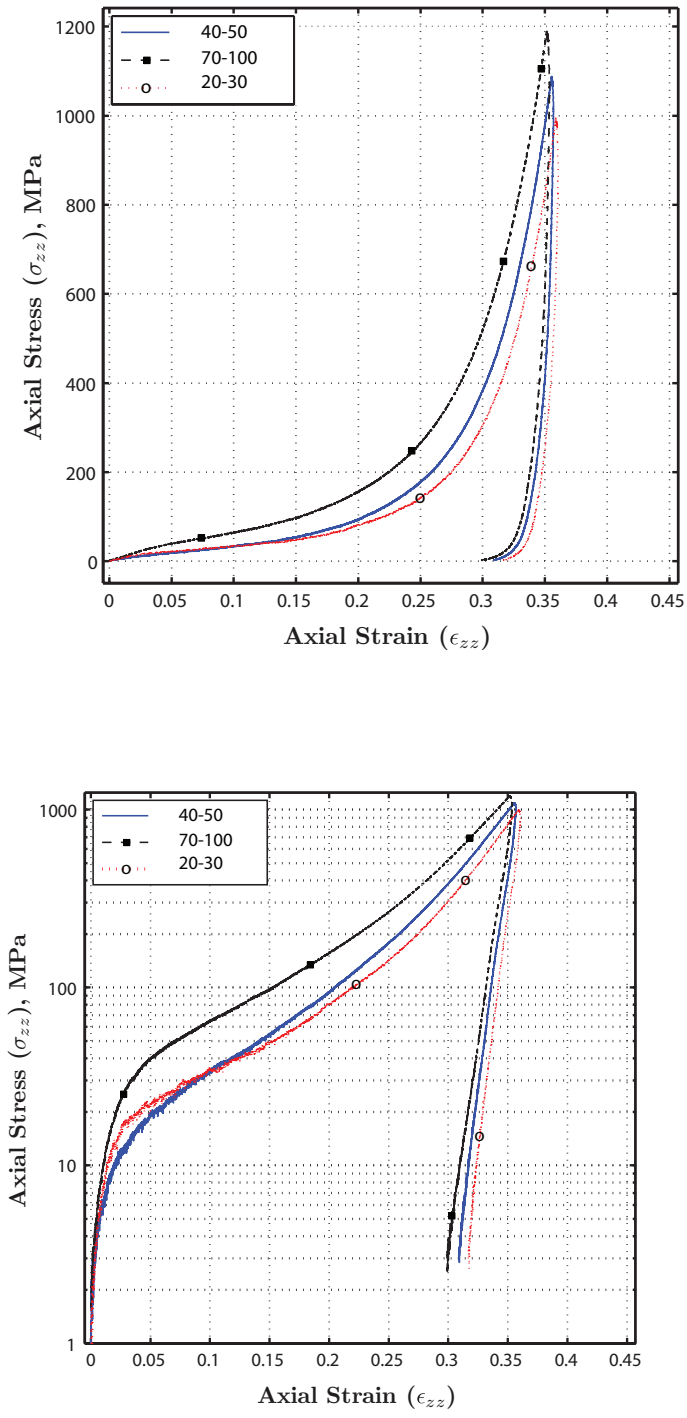

Figure 6.11: Linear and semi-log plot of axial stress vs axial strain for sieve sizes of 100 (fine), 30 (coarse), and Eglin sand at initial density of 1.55 g/cm^3.

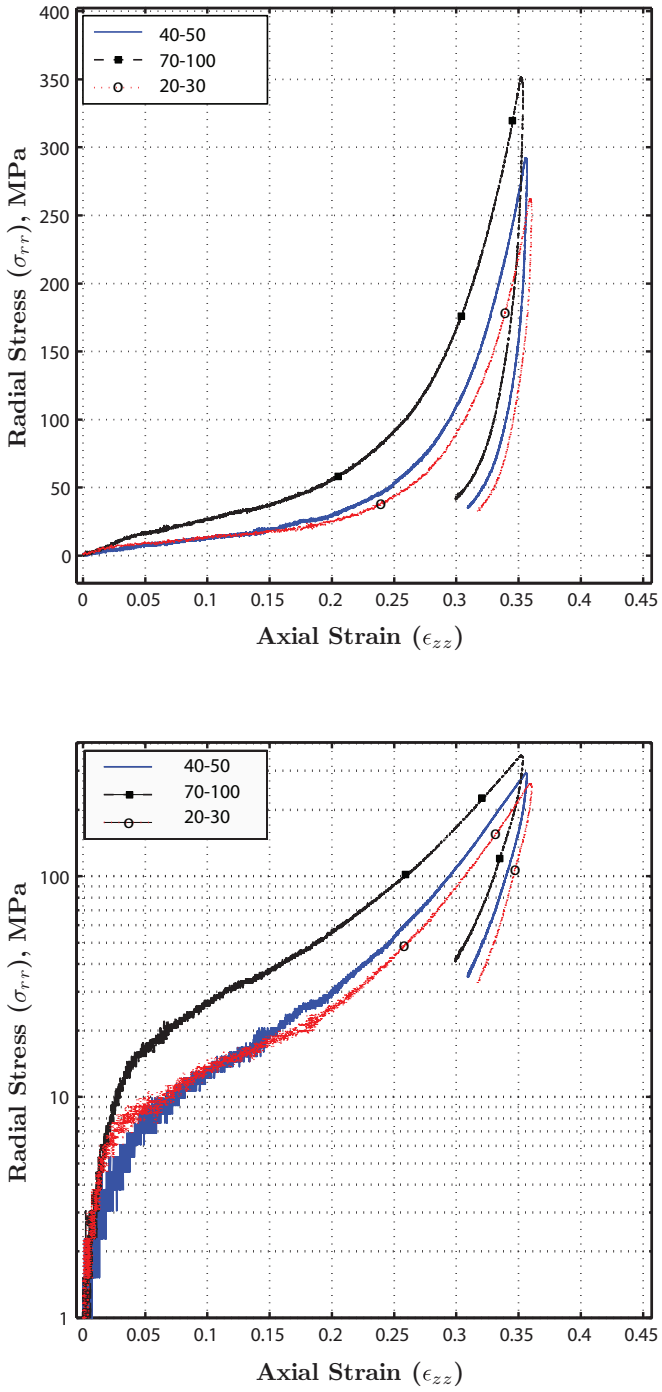

Figure 6.12: Linear and semi-log plot of radial stress vs axial strain for sieve sizes of 100 (fine), 30 (coarse), and Eglin sand at initial density of 1.55 g/cm^3.

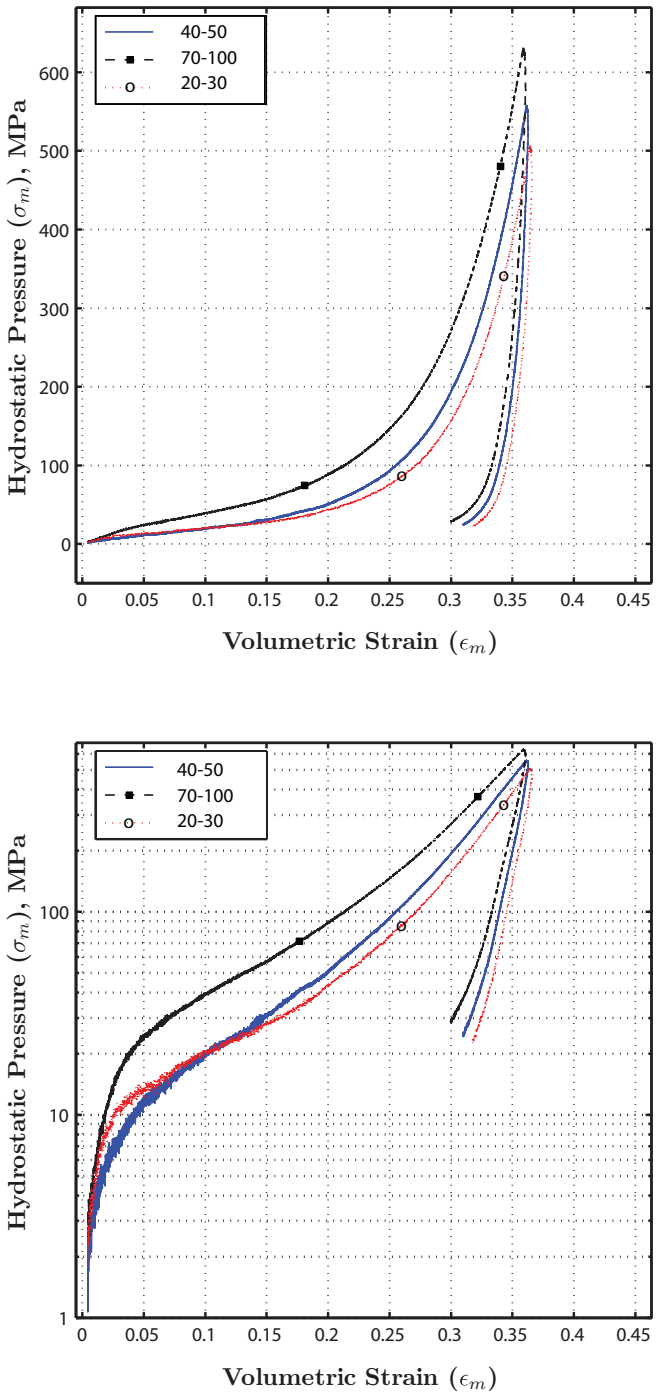

Figure 6.13: Linear and semi-log plot of hydrostatic pressure vs volumetric strain for sieve sizes of 100 (fine), 30 (coarse), and Eglin sand at initial density of 1.55 g/cm^3.

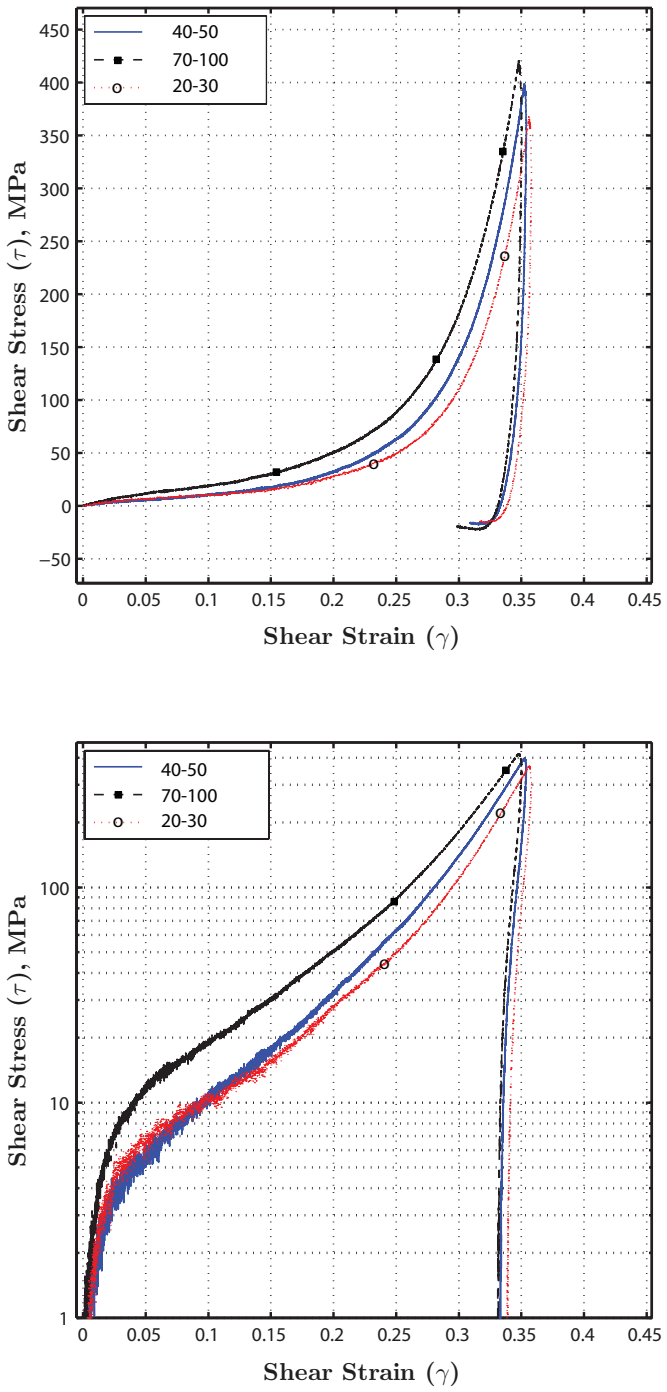

Figure 6.14: Linear and semi-log plot of shear stress vs shear strain for sieve sizes of 100 (fine), 30 (coarse), and Eglin sand at initial density of 1.55 g/cm^3 for initial density of 1.55 g/cm^3.

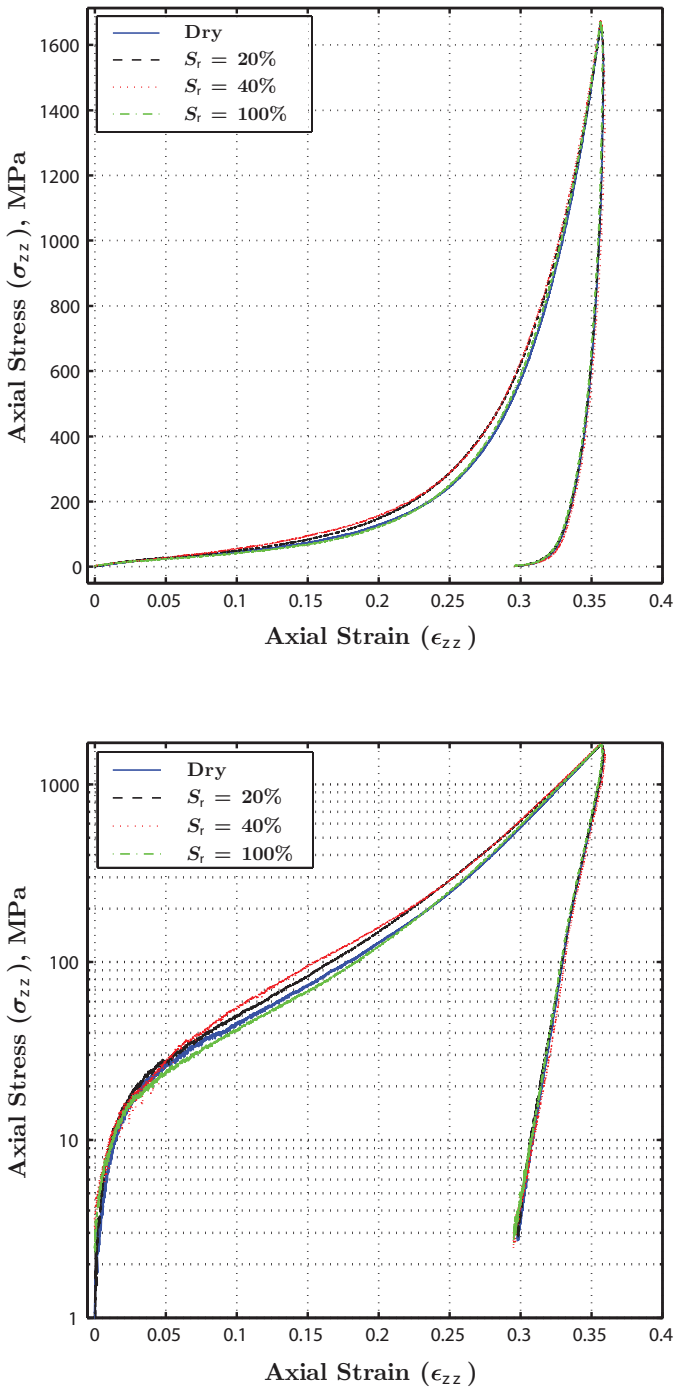

Figure 6.15: Linear and semi-log plot of axial stress vs axial strain for 0%, 20%, 40%, and 100% water saturation.

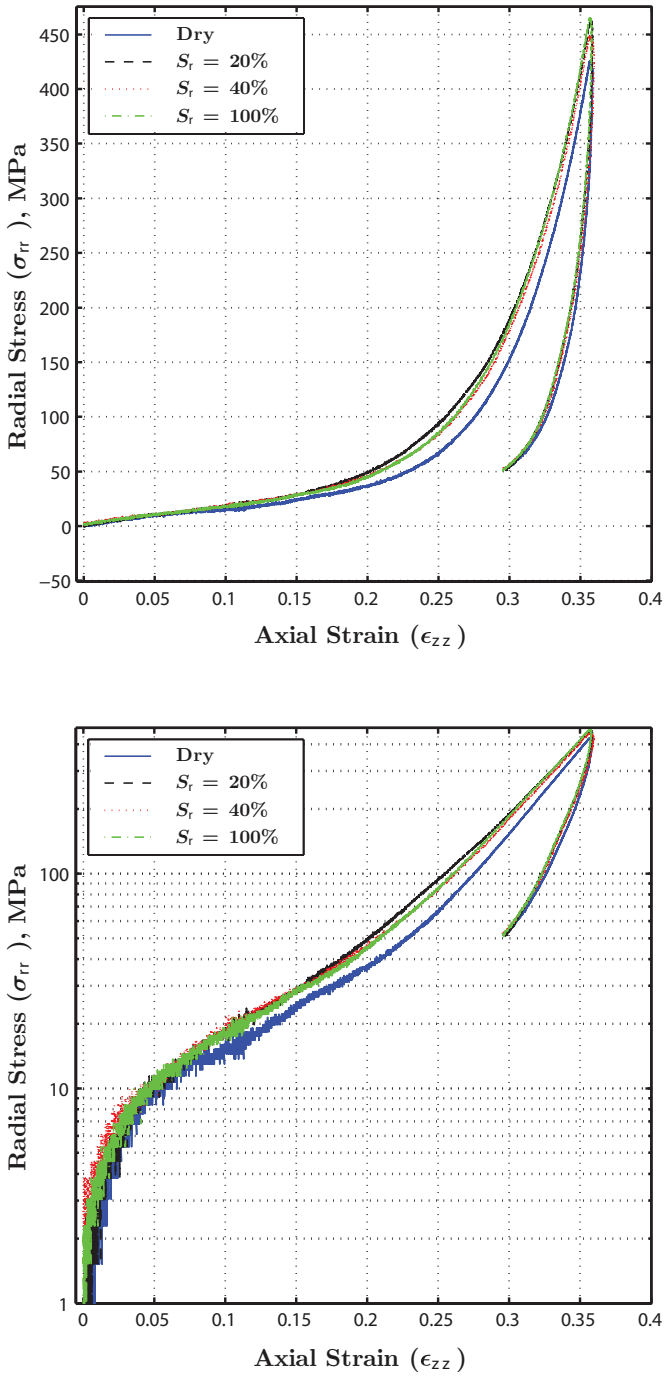

Figure 6.16: Linear and semi-log plot of radial stress vs axial strain for 0%, 20%, 40%, and 100% water saturation.

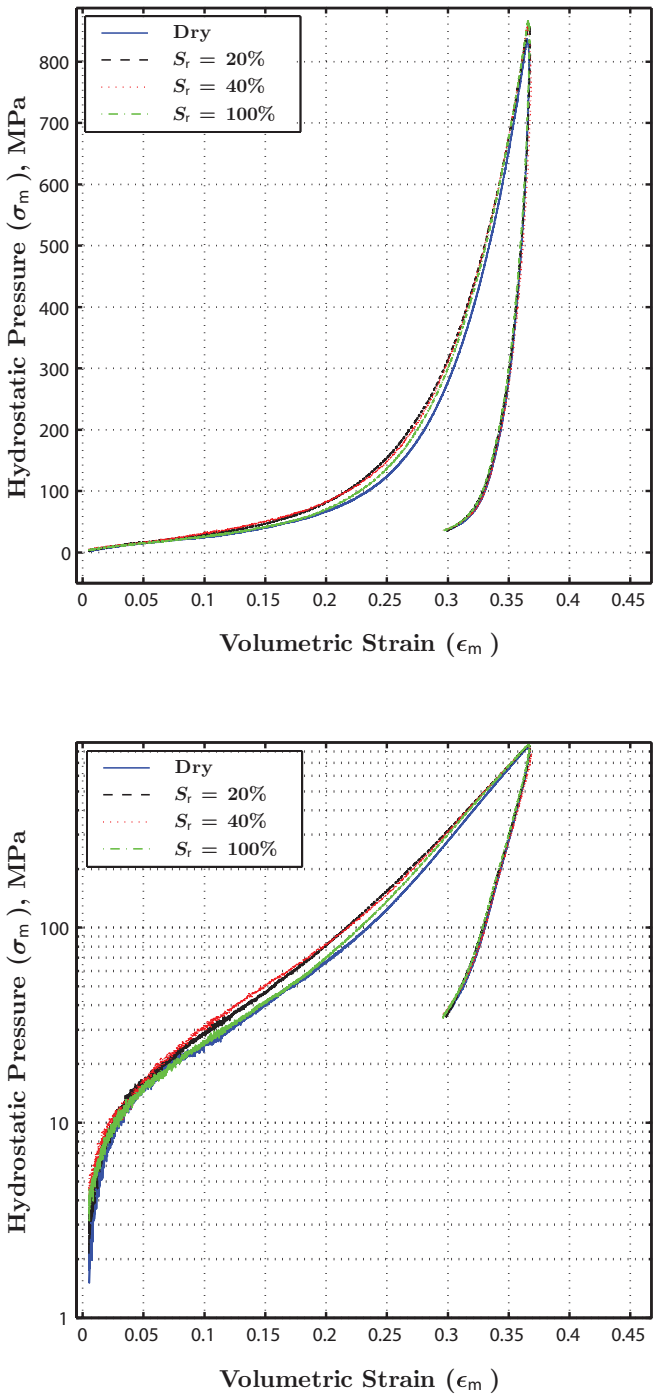

Figure 6.17: Linear and semi-log plot of hydrostatic pressure vs volumetric strain for 0%, 20%, 40%, and 100% water saturation.

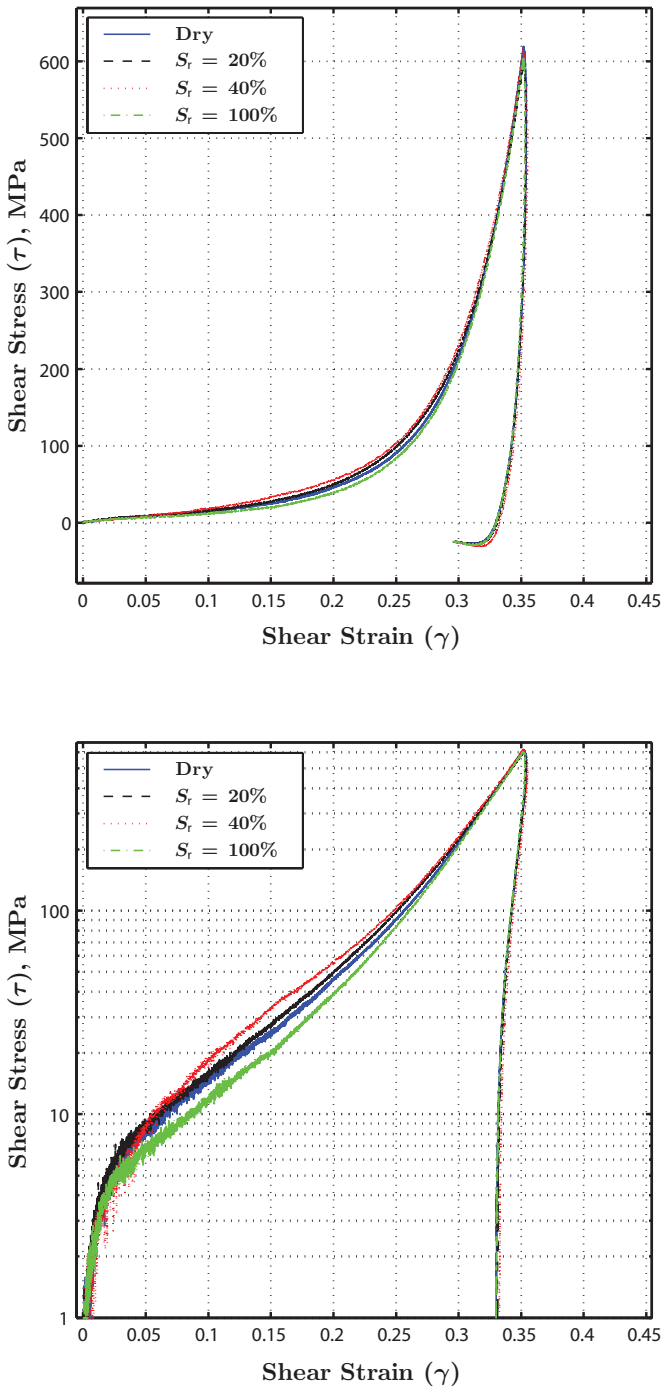

Figure 6.18: Linear and semi-log plot of shear stress vs shear strain for 0%, 20%, 40%, and 100% water saturation.

CHAPTER 7

DISCUSSION

Results of the experiments conducted to investigate the static behavior of Eglin sand in uniaxial compression are presented in the previous chapter. The axial, radial, mean, and shear stress-strain curves for the three parameters tested in this experimental investigation, namely, initial density, particle size, and moisture content are presented in Figures 6.6 through 6.18.

7.1 Effect of initial density

Figures 6.6, 6.7, 6.8, and 6.9 present the axial, radial, mean, and shear stress-strain curves for the densities of 1.55, 1.60, 1.65, and 1.70 g/cm^3. The linear plot of axial stress-strain curves in Figure 6.6 exhibit two linear trends in the loading region followed by a linear unloading curve. The curves follow the general three phase behavior proposed by Hagerty *et al.* [13], as seen in Figure 2.7. The first linearity is observed in the initial portion of the loading curve occurs, between 0% and 0.5% axial strains. Hagerty *et al.* [13] defined

the slope of the initial portion of the loading curve as the secant modulus (M_i). The initial linear slope for the four different densities investigated are found to be same, as seen in Figure 6.6. This is likely due to the elastic compression of the sand grains during initial loading. The slopes of all the curves for different densities of Eglin sand are found to be similar. There is no apparent influence of initial density on the secant modulus.

The initial linear region is terminated at the break-point stress, after which particle crushing begins. This region is marked by a drastic drop in the slope of the stress-strain curve. The axial stress-strain plot shows the dependence of the onset of particle crushing on the initial density. The break-point stress is found to increase with increase in initial density. This is found to be in agreement with the results of Hagerty *et al.* [13] and Hendron [17]. The break-point stress becomes less distinguishable as the initial density increases. In the semi-log curve of axial stress-strain, shown in Figure 6.6, the break-point stress of 1.70 and 1.65 g/cm^3 are very similar, whereas the 1.55, 1.60, and 1.65 g/cm^3 show clear onset of particle crushing.

The crushing and rearrangement of sand particles is found to be gradual in loosely packed sand than in dense sand. The higher packing density of densely packed sand constrain the rearrangement of the sand grains which lead to the build-up of higher stresses. Thus the duration of grain crushing in densely packed sand is shorter than that of loosely packed sands.

The transitional phase of grain crushing is gradually followed by the pseudoelastic compression phase, where the crushed grains behave much stiffer than in the the initial uncrushed phase. Hagerty *et al.* [13] defined the slope of the final pseudoelastic phase as the final constrained modulus (M_f). During the final pseudoelastic phase, the voids are filled with fine comminuted particles and show much higher stiffness. Hence, M_f is found to be much higher than the M_i. Similar trends are observed in the radial, hydrostatic, and shear stress-strain curves.

The unloading phase is marked by a rapid drop in axial stress for small change in axial strain. This indicates a small elastic recovery possibly due from the pseudoelastic compression phase. A small negative slope is seen in the unloading curves of 1.70 g/cm^3 and 1.65 g/cm^3 in Figure 6.6. This behavior might be due to the use of the loading compliance curve for compliance correction, although similar behavior is also observed in the radial stress-strain plots in Figure 6.7. The negative slope indicates an increase in stress during the start of unloading, when the strain is reduced in the sample. It is not clear if this behavior is due to the machine compliance or from the mechanical response of crushed sand. The extent of elastic recovery is similar for all densities, indicating that the elastic strain energy accumulated in the pseudoelastic phase is recovered during unloading.

The trends observed in the axial stress-strain curves in Figure 6.6 agree closely with the previous results obtained by Hagerty *et al.* [13] and Yamamuro *et al.* [32], shown in Figures 2.4, 2.5, 2.6, and 2.9. Overall, the stiffness of the stress-strain curves increased with higher initial density. Dynamic tests conducted by Luo *et al.* [20] on the Split Hopkinson Pressure bar (SHPB) up to axial stresses of 350 MPa, show similar trends in the curves of axial stress-strain.

The semi-log plot of void-ratio versus axial stress in Figure 6.10, is typically used to understand the degree of sand crushing as a function of axial stress in soil mechanics. Densely packed sand has lesser voids than loosely packed sand. The void ratio curve is found to be in agreement with the trend observed in the void ratio curves of Yamamuro *et al.* [32] as seen in Figure 2.10. The initial slope of the semi-log plot shows a linear phase for axial stresses below 10 MPa. This linear phase is followed by rapid collapse of voids with increase in axial stress. The void ratio curves for the different densities are found to unite along a common path. This merging of void ratio curves has been previously reported by Hagerty *et al.* [13] and Yamamuro *et al.* [32]. For densely packed sand, namely, 1.70 and 1.65 g/cm^3, the void ratio curves extended to the negative values at axial stresses above 1 GPa. The presence of negative void ratios is thought to be due to the compression of mineral particles, as noted by Hagerty *et al.* [13].

7.2 Effect of particle size

The results of tests conducted on the effect of particle size on the stress-strain behavior of sand are presented in Figures 6.11 through 6.14. Eglin sand was mechanically separated into coarse and fine grains using sieves. Axial stress-strain curves of coarse sand grains (20-30) and fine sand grains (70-100) are shown in Figure 6.11. The coarse grains attain lower stresses at the maximum axial strain of 35% as compared to the fine sand grains. About 50% by weight of Eglin sand contains particles in the sieve size of 40 through 50. The 20-30 and 70-100 particles constitute 9% and 7% of Eglin sand by weight, respectively.

Test results show that the fine grains exhibit the highest stiffness while the coarse grains show the least stiffness. This is explained by the distribution of stresses between the sand particles, as proposed by Hendron [17]. In coarse sand, the average number of interparticle contacts are higher than that in loosely packed sand. The high interparticle contacts correspond inversely to the stresses arising between the particles. Thus, coarse sand has higher interparticle stresses leading to particle fracture at lower axial stresses. The fracture of sand particles also aid in rearrangement and rotation of sand grains, leading to collapse of voids. Fine grain sand breaks down at higher stresses while coarse grain sand start collapsing at lower stresses. The high stiffness of fine grain sand is due to restricted rearrangement of sand grains and rapid collapse of voids.

The radial, hydrostatic and shear stress-strain curves show similar trends.

7.3 Effect of moisture content

The results of tests conducted to investigate the influence of moisture on the stress-strain behavior of sand are presented in Figures 6.15 through 6.18. The axial stress-strain curves, shown in Figure 6.15, for 0%, 20%, 40%, and 100% saturation of water show overlapping trends. Water is thought to influence the mechanical behavior of sand due to its incompressible nature and due to its lubricating effect by reducing the interparticle shear stresses. Due to the nature of the confinement and WC rod assembly design, water is squeezed through the bottom of the confinement during the test. This prevents the build-up of pore pressure due to water in the voids even in 100% (fully saturated) test cases. The effect of water acting as a lubricant is neither observed.

Dynamic tests conducted by Veyera [31] on the effect of moisture content on sand reported an increase in the stiffness of the axial stress-strain curves with increase in moisture content, as seen in Figures 2.12, 2.13, and 2.14. Recent dynamic SHPB tests conducted by Martin *et al.* [23] reported decrease in stiffness of the axial stress-strain curve with increase in moisture content, as seen in Figure 2.15. Static uniaxial strain tests reported by Martin, observed similar trends in static compression tests.

The presence of friction between the sand sample and the inner walls of

the confinement is a source of concern. Previous investigations by various researchers acknowledged this issue. Yamamuro *et al.* [32] attempted to reduce the friction between the sand and confining walls by lubricating the interface. This lead to alteration in the response of sand. Martin *et al.* [23] noted the difficulty in measuring the sidewall friction. In this investigation, sidewall friction was minimized by reducing the sample length and honing the inner surface of the confinement. The overlapping curves of tests conducted with different saturations of water show the effect of sidewall friction to be negligible.

CHAPTER 8

CONCLUSIONS

An experimental investigation was conducted on the uniaxial stress-strain behavior of Eglin sand up to axial stresses of 3 GPa. Quasistatic tests were conducted to primarily investigate three parameters that affect the behavior of sand, namely, initial density, particle size, and moisture content. An uniaxial compression fixture was developed for the purpose of reaching high axial stresses of 3.2 GPa in the sand sample. Previous studies on the compression of sand were limited to axial stresses of 800 MPa [32]. Triaxial tests on sand were further limited to stresses of 128 MPa. Axial stresses of 3.2 GPa and confining pressures of 800 MPa were attained in this investigation. Results of such high pressure multiaxial tests on sand have not been reported in the literature.

The technique of confined compression, developed by Ravichandar [25], was implemented to obtain the multiaxial bulk properties of sand in hardened steel confinement. A strain gage mounted on the confinement measured the hoop strain arising from the radial expansion of the confined

sand during axial compression. All tests were conducted up to axial strains of 35% at constant strain rate of 0.002 s^{-1}. Compliance correction was performed to eliminate the effect of fixture compliance in the axial strain measurements. Three tests were conducted for each test parameter for repeatability.

Four densities of dry sand, namely, 1.55, 1.60, 1.65, and 1.70 g/cm^3 were investigated up to axial strains of 35%. The results show that dense sand is less compressible than loosely packed sand. The slope of the stress-strain curves show that dense sand exhibit higher stiffness as compared to that of less dense sand. The void ratio curves of different densities merge along a single path as the grain crushing approaches completion.

Tests conducted on coarse and fine sand grains at 1.55 g/cm^3 show a significant effect of particle size on the stress-strain behavior of sand. Fine grain sand showed significantly high stiffness when compared to coarse grain sand.

Four different degrees of moisture saturation were conducted on dry Eglin sand at 1.60 g/cm^3. The multiaxial response of sand showed no significant effect of moisture.

CHAPTER 9

FUTURE WORK

The following are the recommendations for further tests on sand to understand the quasistatic stress-strain behavior:

- The use of an extensometer could eliminate the need for compliance correction. Extensometer measures the axial strains in the specimen directly. The design and mounting of a suitable extensometer on the slippery tungsten carbide rods is however a challenge.
- The effect of confinement material can be investigated by testing confinements of different materials and geometries so as to obtain similar radial stiffness response.
- The role of particle size can be further investigated by mixing sand particles of different sizes in known proportions. The resulting stress-strain behavior can be possibly characterized by the proportion of sand particles by size.
- The effect of aspect ratio on the stress-strain response of sand can be

investigated. The extent of repeatability of the current results can be compared by testing sand samples with different aspect ratios.

Sand is known to undergo high pressure compression in cases such as high velocity penetration of projectiles and explosion sites. These instances are of interest to military, mining, and geotechnical engineering. A complete investigation is necessary to understand the behavior of sand in such cases. An extensive experimental program investigating the static and dynamic response of sand is necessary to understand the bulk behavior of sand. Such investigations also aid in defining and validating numerical techniques aimed at predicting the constitutive behavior of sand. Dynamic compressive behavior of sand can be investigated using a Split Hopkinson Pressure bar (SHPB). The results of such dynamic tests on the different parameters influencing the behavior of sand can be compared with the static tests, to understand the effect of strain rate on sand.

BIBLIOGRAPHY

[1] Standard practice for classification of soils for engineering purposes (unified soil classification system), 2001. Section 4, Volume 04.08.

[2] W.A. Allen, E.B. Mayfield, and H.L. Morrison. Dynamics of a projectile penetrating sand. *Journal of Applied Physics*, 28(3):370–376, 1957.

[3] W.A. Allen, E.B. Mayfield, and H.L. Morrison. Dynamics of a projectile penetrating sand. part ii. *Journal of Applied Physics*, 28(3):370–376, 1957.

[4] E. Blackwelder. The origin of central kansas oil domes. *Bulletin of the American Society of Petroleum Geologists*, 4:89, 1920.

[5] J.P. Borg and T.J. Vogler. Mesoscale simualtions of a dart penetrating sand. *International Journal of Impact Engineering*, 35:1435–1440, 2008.

[6] H.G. Botset and B.W. Reed. Experiment on compressibility of sand. *Bulletin of the American Society of Petroleum Geologists*, 19:1053, 1935.

[7] M. Budhu. *Soil Mechanics And Foundations*. John Wiley & Sons Inc., 2 edition, 2006.

[8] S. Chocron, J.D. Walker, A.E. Nicholls, A.K. Dannemann, and C.E. Anderson Jr. Analytical model of the confined compression test used to characterize brittle materials. *Journal of Applied Mechanics*, 75(2):1–7, 2008.

[9] K.A. Dannemann, A.E. Nicholls, S. Chocron, J.D. Walker, and C.E. Anderson Jr. Compression testing and response of sic n-ceramics:intact, damaged and powder. In *Ceramic Engineering and Science Proceedings, Advances in Ceramic Armor, 29th International Conference on Advanced Ceramics and Composites*, volume 26, pages 109–116, 2005.

[10] J.M. De Souza. Compressibility of sand at high pressure. Master's thesis, Massachusetts Institute of Technology, Cambridge, Massachusetts, 1958.

[11] P. Forquin, A. Arias, and R. Zaera. An experimental method of measuring the confined compression strength of geomaterials. *International Journal of Solids and Structures*, 44(13):4291–4317, 2007.

[12] J. Graham, M. Alfaro, and Ferris; G. Compression and strength of dense sand at high pressures and elevated temperatures. *Canadian Geotechnical Journal*, 41:1206–1212(7), 2004.

[13] M.M. Hagerty, D.R. Hite, C.R. Ullrich, and D.J. Hagerty. One-dimensional high-pressure compression of granular media. *Journal of Geotechnical Engineering*, 119(1):1–18, 1993.

[14] E.B. Hall and B.B. Gordon. Triaxial testing with large-scale high pressure equipment, astm-361, 1963.

[15] E. Hanina, D. Rittel, and Z. Rosenberg. Pressure sensitivity of adiabatic shear banding in metals. *Applied Physics Letters*, 90:3, 2007.

[16] P. Harremoes. Compressibility of ground sand at high pressures. Master's thesis, Massachusetts Institute of Technology, Cambridge, Massachusetts, 1959.

[17] A.J. Hendron. *Behavior of sand in one-dimensional compression*. PhD thesis, University of Illinois, Urbana, Illinois, 1963.

[18] J. Henrych. *The dynamics of explosion and its use*. Elsevier Scientific Publishing Company, Amsterdam, 1979.

[19] H.M. Jaeger, S.R. Nagel, and R.P. Behringer. The physics of granular materials. *Physics Today*, pages 32–38, 1996.

[20] H. Luo, H. Lu, W.L. Cooper, and R. Komanduri. Dynamic compaction of dry sand under confinement at high strain rates. *Unpublished*.

[21] Z. Ma and K. Ravi-Chandar. Confined compression: A stable homogeneous deformation for constitutive characterization. *Experimental Mechanics*, 40(1):38–45, 2000.

[22] B. E. Martin. Moisture effects on the high strain-rate behavior of sand. Master's thesis, University of Florida, 2007.

[23] B.E. Martin, W. Chen, Bo Song, and S. Akers. Moisture effects on the high strain-rate behavior of sand. *Mechanics of Materials*, 41:786–798, 2009.

[24] D.J. Murphy. *Stress, degradation, and shear strength of granular material*. Gulf Publishing Company, Houston, Texas, 1987.

[25] K. Ravi-Chandar and Z. Ma. Inelastic deformation in polymers under multiaxial compression. *Mechanics of Time-Dependent Materials*, 4(4):333–357, 2000.

[26] D. Rittel, E. Hanina, and G. Ravichandran. A note on the direct determination of the confining pressure of cylindrical specimens. *Experimental Mechanics*, 48(3):375–377, 2008.

[27] K. Terzaghi. Elastic behavior of sand and clay. *Engineering News Record*, 95:987, 1925.

[28] K. Terzaghi, R.B. Peck, and G. Mesri. *Soild mechanics in engineering practice*. John Wiley & Sons Inc., 3rd edition, 1996.

[29] S. Timoshenko and J.N. Goodier. *Theory of Elasticity*. McGraw-Hill, New York, 1951.

[30] A.S. Vesic and G.W. Clough. Behavior of granular materials under

high stresses. *Journal of the Soil Mechanics and Foundations Division*, 94(3):661–668, 1968.

[31] G.E. Veyera. Uniaxial stress-strain behavior of unsaturated soils at high strain rates. Technical Report WL-TR-93-3523, Wright-Patterson Air Force base, 1994.

[32] J.A. Yamamuro, P.A. Bopp, and P.V. Lade. One-dimensional compression of sands at high pressures. *Journal of Geotechnical Engineering*, 122(2):147–154, 1996.

APPENDIX A

Terminology

Definitions of some commonly used terms in this study are presented in this chapter [7, 28].

Water content (w): This is the ratio of weight of water (W_w) to the weight of sand (W_s). Water content is usually expressed as percentage. The dry weight of sand is determined by drying the sand in an oven at 110$\pm$5°C until no further change in weight occurs, usually attained in for 24 hours.

$$w = \frac{W_w}{W_s} \times 100\%$$

Void ratio (e): This is the ratio of the volume of voids (V_v) to the volume of sand (V_s). Loose sands have high value of void ratio while dense sands have low void ratio value.

$$e = \frac{V_v}{V_s}$$

Porosity (n): This is the ratio of the volume of voids (V_v) to the total

volume (V).

$$n = \frac{V_v}{V}$$

Porosity (n) and void ratio (e) can be expressed in terms of one another by the following expression:

$$n = \frac{e}{1+e}$$

In the case of perfect spheres, the maximum and minimum achievable porosities are 48% and 26%, respectively. This corresponds to a maximum and minimum void ratios of 0.91 and 0.35, respectively. For natural sands, porosity varies from 25% to 50%.

Degree of saturation (S): This is the ratio of the volume of water to the volume of voids.

$$S = \frac{V_w}{V_v}$$

Dilatancy: Reynolds used the term 'dilatancy' in 1885 to describe the property of granular materials to change in volume as a result of the rearrangement of grains.

APPENDIX B

Processing of Acquired Data

A Matlab m-code created for processing the data obtained from the MTS load frame and the Hoop strain gage. The test data is read from two files; one containing the axial force and displacement data and the other containing the hoop strain. The files are input and the axial force and displacement are converted to corresponding axial stress and strain after compliance correction. The data is then plotted separately and the temporal synchronization of the axial and strain signal is performed by the user. The values of the stresses and strains are then written to a text file for further analysis and plotting. The Matlab code is presented below.

```
% This Matlab code was created by Vijay Subramanian, Mechanical & Aerospace
% Engineering for processing the data obtained from the MTS test frame and
% the hoop strain measurements from the Unixial Tests on Sand.
% This code reads the test files,
% Last modified: 2010-June-29

clear all ;
```

```
clc ;

%fpath = 'ES-Pall-D170-M40-QS' ; Lsample = 7.49 ;
%fname = '-1' ; Delta = (5465 - 4910) ; % Good
%fname = '-2' Delta = (10610 - 10119) ; % Good
%fname = '-3' ; Delta = (10395 - 9852) ; % Good
%fname = '-4' ;  % Good
%ptitle = '\textbf{Dry Eglin sand, $\rho$ = 1.70 g/cm$^3$,
    m =0.40 g}' ;

%fpath = 'ES-Pall-D165-M40-QS' ; Lsample = 7.72 ;
%fname = '-1' ;  %
%fname = '-2' ;  %
%fname = '-3' ;  % Good

%fpath = 'ES-Pall-D165-M40-QS' ; Lsample = 7.72 ;
%fname = '-4' ; % Good
%fname = '-5' ; Delta = 0 ;% Good
%fname = '-6' ; Delta = (10175 - 9272) ; % Good
%ptitle = '\textbf{Dry Eglin sand, $\rho$ = 1.65 g/cm$^3$,
    m =0.40 g}' ;

%fpath = 'ES-Pall-D160-M40-QS' ; Lsample = 7.96 ;
%fname = '-1' ; %
%fname = '-2' ; %
%fname = '-3' ; %
%fname = '-4' ; %
%fname = '-5' ; %
%fname = '-6' ; Delta = (9449 - 8861) ;  % Good
%fname = '-7' ; Delta = (10456 - 8865) ;  % Good
%fname = '-8' ;Delta = (10021 - 8856) ;  % Good
%ptitle = '\textbf{Dry Eglin sand, $\rho$ = 1.60 g/cm$^3$,
    m =0.4000 g}' ;

%fpath = 'ES-Pall-D160-M40-H5-QS' ; Lsample = 7.96 ;
%ptitle = '\textbf{Eglin sand, $\rho$ = 1.60 g/cm$^3$, $w$
    = 5\%, $S_r$ = 20\%, m =0.40g}' ;
%fname = '-1' ; Delta = (10130 - 8866)  ;  %
%fname = '-2' ; Delta = (10580 - 8864);
%fname = '-3' ; Delta = (0 - 0) ;

%fpath = 'ES-Pall-D160-M40-H10-QS' ; Lsample = 7.96 ;
```

```
%ptitle = '\textbf{Eglin sand, $\rho$ = 1.60 g/cm$^3$, $w$
    = 10\%, $S_r$ = 40\%, m =0.40g}' ;
%fname = '-1' ; Delta = (10130 - 8866)  ;  %
%fname = '-2' ; Delta = (0 - 0)  ;  %
%fname = '-3' ; Delta = (0 - 0)  ;  % Good
%fname = '-4' ; Delta = (0 - 0)  ;  %
%fname = '-5' ; Delta = (960)  ;  % Good
%fname = '-6' ; Delta = (1920)  ; % Good
%fname = '-2' ;
%fname = '-3' ;

%fpath = 'ES-Pall-D160-M40-H100-QS' ; Lsample = 7.96 ;
%ptitle = '\textbf{Eglin sand, $\rho$ = 1.60 g/cm$^3$, $w$
    = 25\%, $S_r$ = 100\%, m =0.40g}' ;
%fname = '-1' ; Delta = (0 - 0)  ;  %
%fname = '-2' ; Delta = (0 - 0);
%fname = '-3' ; Delta = (560) ;

% fpath = 'ES-Pall-D170-H10-M40-QS' ; Lsample = 7.49 ;
% ptitle = '\textbf{Eglin sand, $\rho$ = 1.70 g/cm$^3$,
   $w$ = 10\%, m =0.40g}' ;
%fname = '-1' ; Delta = (10130 - 8866)  ;  %
%fname = '-2' ; Delta = (10580 - 8864);
% fname = '-3' ; Delta = (0 - 0) ;

%fpath = 'ES-Pall-D155-M40-QS' ;  Lsample = 8.21 ; %
%fname = '-1' ;
%fname = '-2' ;
%fname = '-3' ;
%fname = '-4' ;
%fname = '-6' ; Delta = (10217 - 8577) ;  % Good
%fname = '-7' ; Delta = (10016 - 8580) ;  % Good
%fname = '-8' ; Delta = (11029 - 8568) ;  % Good
%ptitle = '\textbf{Dry Eglin sand, $\rho$ = 1.55 g/cm$^3$,
    m =0.4000 g}' ;

%fpath = 'ES-P100-D155-M40-QS' ; Lsample = 8.21 ;
%fname = '-1' ; Delta = (9328 - 8573) ;  % Good
%fname = '-2' ; Delta = (10015 - 8584) ;  % Good
%fname = '-3' ;  Delta = (9667 - 8573) ;  % Good
%ptitle = '\textbf{Dry Eglin sand (Sieve\#100), $\rho$ =
   1.55 g/cm$^3$, m =0.4000 g}' ;
```

```
fpath = 'ES-P30-D155-M40-QS' ;  Lsample = 8.21 ;
fname = '-1' ; Delta = (9521 - 8578) ;  % Good
fname = '-2' ; Delta = (10427 - 8574) ;  % Good
fname = '-3' ;  Delta = (9442 - 8579) ;  % Good
ptitle = '\textbf{Dry Eglin sand (Sieve\#30), $\rho$ = 1.55 g/cm$^3$, m =0.4000 g}' ;


dir = ['F:\SandComp\data\',fpath,'\',fpath,fname,'\'] ;
filename1 = [fpath,fname,'.csv'] ;
filename2 = 'CH1#00001_01h.TXT' ;
filename3 = 'CH2#00001_02h.TXT' ;

fileToRead1=[dir,filename1] ;
newData1 = importdata(fileToRead1);
% Create new variables in the base workspace from those fields.
vars = fieldnames(newData1);
for i = 1:length(vars)
    assignin('base', vars{i}, newData1.(vars{i}));
end

ch1 = data(:,1) ; % time,s (freq = 50 Hz)
ch2 = data(:,2) ; % command sig or syncA signal
ch3 = data(:,3) ; % position, mm
% ch4 = load, kN
if data(1,4) > 0.01 ; ch4 = -data(:,4) ;
else ch4 = -data(:,4)-data(1,4); end % initializing ch4 data/load to zero
%ch5 = data(:,5) ; % extensometer position, mm

DELIMITER = '\t';
HEADERLINES1 = 13;
% Import the file containing HOOP Strain data
newData2 = importdata([dir filename2],DELIMITER, HEADERLINES1);
% Create new variables in the base workspace from those fields.
vars = fieldnames(newData2);
for i = 1:length(vars)
    assignin('base', vars{i}, newData2.(vars{i}));
```

```
end
ch6 = data ; % hoop strain data, V

% Import the file containing Sync signal B
newData3 = importdata([dir filename3],DELIMITER, ↩
   HEADERLINES1);
% Create new variables in the base workspace from those ↩
   fields.
vars = fieldnames(newData3);
for i = 1:length(vars)
    assignin('base', vars{i}, newData3.(vars{i}));
end
ch7 = data ; % synchronizing signal from Instron ↩
   controller to oscilloscope, V

syncA = abs(ch2 - ch2(1)) ; % syncA signal
syncB = abs(ch7 - ch7(1)) ; % syncB signal

% finding the START point of loading
% by finding the index when load exceeded 0.0400 kN
i = 1 ;
while ch4(i) < 0.04 && i < length(ch4)
    i = i+1 ;
end
stval = i ;

% finding the END point of loading
% by finding the index when load went below 0.0400 kN
i = length(ch4) ;
while ch4(i) < 0.10 && i > 1
    i = i-1 ;
end
endval = i ; % The loading ends after this array index.

% detecting the edge of the loading curve
% by finding the index of when the load goes to max load.
i = length(ch4) ;
while ch4(i) < max(ch4) && i > 1
    i = i-1 ;
end
loadval = i ; % The loading ends after this array index.
%%
```

```
t50 = ch1(stval:endval)-ch1(stval) ; % time sampled at 50 Hz
Fzz = ch4(stval:endval)  ; % axial force from load cell, kN

cmdsig = ch2(stval)-ch2(stval:endval) ;
ucgdzz = ch3(stval)-ch3(stval:endval) ; % uncorrected global displacement, mm
%sdzz = (ch5(stval)-ch5(stval:endval))/ch5(stval) ; % sample strain

cd 'F:\SandComp\Compliance\ComplianceTest-6\' ;

complianceval = Fzz * 0 ;
gdzz = Fzz * 0 ;
for i = 1 : length(Fzz)
    if i <= loadval
        corrtype = 1 ; % 1 = Loading
    else
        corrtype = 2 ; % 2 = Unloading
    end

    complianceval(i) = compliancecalc(corrtype,Fzz(i)) ; % value of compliance
    gdzz(i) =  ucgdzz(i) - complianceval(i) ;
end

a = gdzz(1) ;
gdzz = gdzz - gdzz(1) ;

Arod = pi()*(6.34^2)/4 ; % Area of WC rod , mm2
Asigmazz = Fzz * 1e3 / Arod ; % Axial Stress, MPa
ucepsilonzz = ucgdzz / Lsample ; % uncorrected strain
epsilonzz = gdzz / Lsample ; % strain corrected using loading compliance

% 4) Processing the data from Hoop strain gage
t100 = ch4 * 0 ;
epsilonh100 = t100 * 0 ;
epsilonh = t100 * 0 ;
strainh = t100 * 0 ;
for i = 1 : length(ch6) %
```

```
    t100(i) = (1/100)*(i-1) ; % time in seconds
    epsilonh100(i) = 4 * (ch6(i)-ch6(1))/(2.08*15*100); % Hoop Strain
end

% Reducing the 100 Hz data to 50 Hz in Hoop strain measurements
for i = 1 : length(epsilonh100)/2 %
    epsilonh(i) = epsilonh100(2*i-1) ;
end

Ec= 190 *1e3 ; % Young's modulus of confinement, Mpa
epsilonrr =  epsilonh * ((1-0.3)+(1+0.3)*2^2)/2  ; % Radial Strain
Asigmarr = ((2^2-1)*Ec *epsilonh / 2) ; % Radial Stress, MPa
%Asigmarr100 = ((2^2-1)*Ec *epsilonh / 2) ; % Radial Stress, MPa

%% Plotting the force-displacement curve
LL = 1;
UL = length(Fzz) ;
% Plot 1 data - Loading curve
y1data = Fzz(LL:UL) ;
x1data = ucgdzz((LL:UL)) ;
L1style = 'b-' ;
% Plot 2 data
y2data = Fzz(LL:UL) ;
x2data = gdzz((LL:UL)) ;
L2style = 'r-' ;
% Axis limits
ymin = min(y1data)-5;
ymax = max(y1data)+5;
xmin = min(x1data)-0.1;
xmax = max(x1data)+0.1;
% Plot attributes
Lwidth = 1.5 ;
ylabeltext = '\textbf{Axial Force ($F_{zz}),$ kN}' ;
xlabeltext = '\textbf{Axial Displacement, mm}' ;
opfilename = 'force-disp';
% plot legend
legYorN = 'Y' ;
```

```
legA = 'Global displacement' ;
legB = 'Corrected displacement' ;
cd 'F:\SandComp\processor' ;
my2axisplot1(x1data,y1data,L1style,x2data,y2data,L2style,...
   Lwidth,xmin,xmax,ymin,ymax,xlabeltext,ylabeltext,ptitle...
   ,dir,opfilename,legYorN,legA,legB);

% Plotting the Axial Stress vs Axial Strain
LL = 1;
UL =length(Fzz) ;
%UL = length(Fzz) ;
% Plot 1 data - Loading curve
y1data = Asigmazz(LL:UL) ;
x1data = epsilonzz((LL:UL)) ;
L1style = 'b-' ;
% Plot 2 data
y2data = Asigmazz(LL:UL) ;
x2data = ucepsilonzz(LL:UL) ;
%x2data = epsilonzz((LL:UL)) ;
L2style = 'r-' ;
% Axis limits
ymin = min(y2data)-5;
ymax = max(y2data)+50;
xmin = min(x2data)-0.005;
xmax = max(x2data)+0.005;
% Plot attributes
Lwidth = 1.5 ;
ylabeltext = '\textbf{Axial Stress ($\sigma_{zz}),$ MPa}' ...
   ;
xlabeltext = '\textbf{Axial Strain ($\epsilon_{zz})$}' ;
%ptitle = '\textbf{Dry Eglin sand, $\rho = 1.55 g/cm^3$, m...
    =0.40 g}' ;
opfilename = 'Axialstress-strain';
% plot legend
legYorN = 'Y' ;
legA = 'Corrected Strain' ;
legB = 'Uncorrected Strain' ;
cd 'F:\SandComp\processor' ;
my2axisplot1(x1data,y1data,L1style,x2data,y2data,L2style,...
   Lwidth,xmin,xmax,ymin,ymax,xlabeltext,ylabeltext,ptitle...
   ,dir,opfilename,legYorN,legA,legB);
```

```
% Plotting the Axial stress vs time
LL = 1;
UL = length(t50) ;
% Plot 1 data - Loading curve
y1data = Asigmazz(LL:UL) ;
x1data = t50(LL:UL) ;
L1style = 'b-' ;
% Axis limits
ymin = min(y1data)-50;
ymax = max(y1data)+50;
xmin = min(x1data)-0.01;
xmax = max(x1data)+0.01;
% Plot attributes
Lwidth = 1.5 ;
ylabeltext = '\textbf{Axial Stress ($\sigma_{zz}$), MPa}' ;
xlabeltext = '\textbf{Time, s}' ;
%ptitle = 'Dry Eglin sand, $\rho = 1.70 g/cm^3$, m =0.40g' ;
opfilename = 'axialstress-time';
cd 'F:\SandComp\processor' ;
my1axisplot1(x1data,y1data,L1style,Lwidth, xmin,xmax,ymin, ymax, xlabeltext,ylabeltext,ptitle,dir,opfilename)

% Plotting the radial stress vs time

LL = 1;
UL = length(Asigmarr) - 100 ;

t = 0 * Asigmarr ;
for i = 1 : UL
    t(i) = (1/50)*i ;
end

% Plot 1 data - Loading curve
y1data = Asigmarr(LL:UL) ;
x1data = t(LL:UL) ;
L1style = 'b-' ;
% Axis limits
ymin = min(y1data)-50;
ymax = max(y1data)+50;
xmin = min(x1data)-0.01;
```

```
xmax = max(x1data)+0.01;
% Plot attributes
Lwidth = 1.5 ;
ylabeltext = '\textbf{Radial Stress ($\sigma_{rr}),$ MPa}' ;
xlabeltext = '\textbf{Time, s}' ;
%ptitle = 'Dry Eglin sand, $\rho = 1.70 g/cm^3$, m =0.4000 g' ;
opfilename = 'radialstress-time';
cd 'F:\SandComp\processor' ;
my1axisplot1(x1data,y1data,L1style,Lwidth, xmin,xmax,ymin, ymax, xlabeltext,ylabeltext,ptitle,dir,opfilename)

%% Plot of synchronizing Axial Stress and Radial Stress vs time

LL = 1 ;
UL = length(Fzz);
Delta = (560);

%_____________________________
% Plot 1 data
x1data = t50(LL:UL) ;
y1data = Asigmazz(LL:UL) ;
L1style = 'b-' ;
% Plot 2 data
x2data = t50(LL:UL) ;
y2data = Asigmarr(LL+Delta:UL+Delta)*max(Asigmazz)/max(Asigmarr(LL+Delta:UL+Delta)) ;
L2style = 'r-' ;
% Axis limits
xmin = min(x1data)-5 ;
xmax = max(x1data)+5 ;
ymin = min(y1data)-20 ;
ymax = max(y1data)+50 ;
%_____________________________
% Plot attributes
Lwidth = 0.5 ;
xlabeltext = '\textbf{Time, s}' ;
ylabeltext = '\textbf{Stress, MPa}' ;
opfilename = 'Axial-RadialStress-Time' ;
% plot legend
```

```
legYorN = 'Y' ;
legA = 'Axial Stress' ;
legB = 'Radial Stress' ;
%_____________________________
cd 'F:\SandComp\processor' ;
my2axisplot1(x1data,y1data,L1style,x2data,y2data,L2style,...
   Lwidth,xmin,xmax,ymin,ymax,xlabeltext,ylabeltext,ptitle...
   ,dir,opfilename,legYorN,legA,legB)

%% Output the variables to an xls sheet.

zz= UL ;

y = [t50(1:zz) Fzz(1:zz) ucgdzz(1:zz) gdzz(1:zz) Asigmazz...
   (1:zz) epsilonzz(1:zz) Asigmarr(1+Delta:zz+Delta) ...
   epsilonrr(1+Delta:zz+Delta)] ; % Asigmarr(1+Delta:zz+...
   Delta)  epsilonrr(1+Delta:zz+Delta)] ;
xlswrite ([dir,fpath,fname], y) ; %
% open the file with write permission
 fid = fopen([dir,fpath,fname,'data.txt'], 'w');
 for i =1 : zz
     fprintf(fid, '%12.8f %12.8f %12.8f %12.8f %12.8f ...
        %12.8f %12.8f %12.8f  \n', [y(i,1) y(i,2) y(i,3) y...
        (i,4) y(i,5) y(i,6) y(i,7) y(i,8)] ) ;
 end
 fclose(fid);
```

A user-defined function was created to plot the data and export the plots to various image formats of Encapsulated Post Script (EPS), Tagged Image File Format (TIFF) and Portable Document Format (PDF).

```
% My matlab plot function to plot 2 data trends
% Created by Vijay Subramanian, OSU, 2010-06-25
%
% x1data = x1-axis data
% y1data = y1-axis data
% x2data = x2-axis data
% y2data = y2-axis data
% l1style = line1 style, 'b-'
% l2style = line2 style, 'r-'
% lwidth = line width, 1.5
% xlabeltext
% ylabeltext
% plottitle
% dir = name of directory
% opfilename = output file name
%
function my2axisplot1(x1data,y1data,L1style,x2data,y2data,...
   L2style,Lwidth,xmin,xmax,ymin,ymax,xlabeltext,...
   ylabeltext,ptitle,dir,opfilename,legYorN,legA,legB)
    figure ;
    plot(x1data,y1data,L1style, x2data,y2data,L2style ,'...
       LineWidth',Lwidth);
    hold on;
    get(gcf)
    get(gca)
    axis square ;
    axis([xmin,xmax,ymin,ymax]); % axis limits
    set(gca,'Color',[1 1 1]*1.00);
    set(gca,'LineWidth',1.5);
    set(gca,'box','on');
    set(gca,'FontName','Arial','FontWeight','b','FontSize'...
       ,12);

    xlabh = get(gca,'XLabel');
```

```
    set(xlabh,'Position',get(xlabh,'Position') - [0.00 ↩
       0.020 0]) ;
    ylabh = get(gca,'YLabel');
    set(ylabh,'Position',get(ylabh,'Position') - [0.10 ↩
       0.000 0]) ;

    xlabel(xlabeltext,'Interpreter','latex','FontName','↩
       Arial','FontWeight','bold','FontSize',15);
    ylabel(ylabeltext,'Interpreter','latex','FontName','↩
       Arial','FontWeight','bold','FontSize',15);
    title(ptitle,'Interpreter','latex','FontName','Arial',↩
       'FontWeight','bold','FontSize',15);
    if legYorN == 'Y'
        h = legend(legA,legB,2);
        set(h,'Interpreter','latex','FontName','Arial','↩
           FontWeight','bold','FontSize',12) ;
    end
    hold off;
    print('-depsc','-tiff','-r300',[dir,opfilename]);
    print('-dpdf','-r300',[dir,opfilename]);
    print('-dtiff','-r300',[dir,opfilename]);
```

Name: Vijay Krishnan Subramanian Date of Degree: December, 2010

Institution: Oklahoma State University Location: Stillwater, Oklahoma

Title of Study: QUASI-STATIC COMPRESSION OF GRANULAR MATERIALS (SAND) AT HIGH PRESSURES ($\sim$ 3 GPA)

Pages in Study: 115 Candidate for the Degree of Master of Science

Major Field: Mechanical Engineering

This investigation presents the results on the static behavior of confined sand (from Eglin Air Force Base) subjected to axial compressive stresses up to 3 GPa. A self-aligning compression fixture was developed to statically compress sand specimen in a cylindrical steel confinement using tungsten carbide pins. A strain gage was mounted on the confining cylinder to measure the circumferential strain. Using axial stress, axial strain, and hoop strain the multi axial behavior of the confined sand is investigated. Compressive tests were conducted up to axial strains of 35%. The static response of the dry sand was tested at four different initial densities, namely, 1.55, 1.60, 1.65, and 1.75 g/cm^3. Effects of particle size, primarily classified as coarse and fine, were investigated. The effect of moisture was also investigated at four different degrees of saturation, namely, 0%, 20%, 40%, and 100%. The dense sand provided a much stiffer response than the loosely packed ones. The coarse sand grains showed significant crushing of particles followed by compaction of the powdered grains.

ADVISOR'S APPROVAL: _____